

THE REGULARIZED MONOTONICITY METHOD: DETECTING IRREGULAR INDEFINITE INCLUSIONS*

HENRIK GARDE[†] AND STRATOS STABOULIS[‡]

Abstract. In inclusion detection in electrical impedance tomography, the support of perturbations (inclusion) from a known background conductivity is typically reconstructed from idealized continuum data modelled by a Neumann-to-Dirichlet map. Only few reconstruction methods apply when detecting indefinite inclusions, where the conductivity distribution has both more and less conductive parts relative to the background conductivity; one such method is the monotonicity method of Harrach and Ullrich. We formulate the method for irregular indefinite inclusions, meaning we make no regularity assumptions on the conductivity perturbations nor on the inclusion boundaries. We show, provided that the perturbations are bounded away from zero, that the outer support of the positive and negative parts of the inclusions can be reconstructed independently. Moreover, we formulate a regularization scheme that applies to a class of approximative measurement models, including the Complete Electrode Model, hence making the method robust against modelling error and noise. In particular, we demonstrate that for a convergent family of approximative models there exists a sequence of regularization parameters such that the outer shape of the inclusions is asymptotically exactly characterized. Finally, a peeling-type reconstruction algorithm is presented and, for the first time in literature, numerical examples of monotonicity reconstructions for indefinite inclusions are presented.

Key words. electrical impedance tomography, indefinite inclusions, monotonicity method, inverse problems, direct reconstruction methods, complete electrode model

AMS subject classifications. 35R30, 35Q60, 35R05, 65N21

1. Introduction. In *electrical impedance tomography* (EIT), internal information about the electrical conductivity distribution of a physical object is reconstructed from current and voltage measurements taken at surface electrodes. More precisely, by prescribing currents in a basis of current patterns and measuring the corresponding voltage, the current-to-voltage map can be obtained. By partly solving the ill-conditioned *Inverse Conductivity Problem*, information about the conductivity, such as the locations and shapes of inclusions in a known background, can be determined. Examples of applications include monitoring patient lung function, control of industrial processes, non-destructive testing of materials, and locating mineral deposits [2, 6, 12, 34, 17, 1, 35, 25, 24].

The governing equation for mathematical models of EIT is the *conductivity equation*

$$(1.1) \quad \nabla \cdot (\gamma \nabla u) = 0, \quad \text{in } \Omega,$$

where $\Omega \subset \mathbb{R}^d$ describes the spatial dimensions of the object, γ is the conductivity distribution, and u is the electric potential. The conductivity equation (1.1) describes the physical interplay of the conductivity and the electric potential under a static electric field. In the *continuum model* (CM), the current-to-voltage map is modelled by a *Neumann-to-Dirichlet* (ND) map $\Lambda(\gamma)$ which relates any applied current density at the boundary to the boundary potential $u|_{\partial\Omega}$ determined through (1.1) and a Neumann condition. In general, unique and stable determination of inclusions has

*This research is funded by grant 4002–00123 *Improved Impedance Tomography with Hybrid Data* from The Danish Council for Independent Research | Natural Sciences.

[†]Department of Mathematical Sciences, Aalborg University, 9100 Aalborg, Denmark.

[‡]Eniram Oy (A Wärtsilä company), Itälahdenkatu 22a, 00210 Helsinki, Finland.

only been rigorously proven for the CM whereas unique solvability results are typically out of reach when using realistic finite dimensional electrode models. Nevertheless, it is possible to obtain reasonable approximations to the inclusions using practically relevant electrode models [9, 16, 28]; to get meaningful reconstructions it is essential to associate the approximate solution to the ideal reconstruction determined by the CM, for instance through regularization theory.

So far, EIT algorithms for inclusion detection have primarily been implemented for the reconstruction of *definite* inclusions, meaning that the conductivity has either only positive or only negative perturbations to the background conductivity. Reconstruction methods for definite inclusions mainly comprise, for instance, the *monotonicity method* [15, 32, 31, 9, 16, 7, 14], the *factorization method* [4, 5, 26, 13, 28, 27], and the *enclosure method* [21, 22, 23, 3]. In this paper we focus on *indefinite* inclusions which consist of both positive and negative perturbations relative to the background conductivity. Only a few theoretical identifiability results exist for the indefinite case. For example, in the factorization method [29, 11] it is required that the domain can be partitioned into two components: one containing the positive inclusions and another the negative ones. The most general result concerns the monotonicity method. It has been shown that there is no need to a priori partition the domain into positive and negative components [15].

The main idea behind the monotonicity method can be illustrated by a simple example. Suppose the conductivity is of the form $\gamma = 1 + \chi_{D_+} - \frac{1}{2}\chi_{D_-}$, where χ_{D_+} and χ_{D_-} are characteristic functions on the open and disjoint sets $D_+, D_- \subseteq \Omega$ that constitute the unknown indefinite inclusion $D = D_+ \cup D_-$ that we wish to reconstruct. For any measurable $C \subseteq \overline{\Omega}$ we have by monotonicity that $D \subseteq C$ implies $\Lambda(1 + \chi_C) \leq \Lambda(\gamma) \leq \Lambda(1 - \frac{1}{2}\chi_C)$. Recently, it was shown that the converse holds if C is closed and has connected complement [15]: If \mathcal{M} is the collection of all such sets C satisfying the above inequalities, then $\cap \mathcal{M}$ characterizes the outer support of D by coinciding with the smallest closed set containing D and having connected complement. In particular, if D has no holes, then the reconstruction coincides with \overline{D} . Remarkably, the result remains valid when replacing the operator inequality with the affine approximation $\Lambda'(1)\chi_C \leq \Lambda(\gamma) - \Lambda(1) \leq -\Lambda'(1)\chi_C$. In practice the affine formulation transforms into fast numerical implementations that mostly rely on cheap matrix-vector products.

In the recent paper [9] a regularized version of the monotonicity method for definite inclusions was studied and asymptotically tied with electrode modelling. In this paper's main result Theorem 3.1 we extend the theory from definite inclusions to indefinite inclusions. We show that a sequence of discrete models that approximate the CM controllably provides a sequence of monotonicity reconstructions that converge to the CM counterpart as the measurement noise and modelling error tend to zero. In particular, it can be shown that favourable approximative models include the *Complete Electrode Model* (CEM) [30, 20] which takes the shunting effect and imperfect electrode contacts into account.

For the CM we extend the results in [15] by showing that non-smooth L^∞ -perturbations are allowed and that they satisfy the required *definiteness condition* as long as the perturbations are essentially bounded away from an underlying piecewise analytic background conductivity. Since we consider L^∞ -perturbations and do not take any regularity assumptions for the boundaries of the inclusions, we call the inclusions *irregular*. Furthermore, we prove in Theorem 2.6 that if the outer boundary of the positive and negative parts of the inclusions can be connected to the domain

boundary by only traversing the background conductivity, then the positive and negative inclusions can be reconstructed independently of one another. A reconstruction algorithm is presented and, for the first time, examples of numerical reconstruction are given for the monotonicity method for indefinite inclusions.

The paper is organized as follows. In Section 2.1 we introduce the CM and give the essential monotonicity properties of the ND map and its Fréchet derivative. The monotonicity method for the CM is outlined in Section 2.2. In particular, Theorem 2.4 gives a simple proof of the method for irregular indefinite inclusions thus forming the main framework of the paper. The proof also enables expressing the conditions under which the positive and negative part of the inclusions can be reconstructed separately; the related results are stated and proven in Theorem 2.6. In Section 3 the regularized monotonicity method is formulated and the main result Theorem 3.1 of the paper is proven. The regularized monotonicity method is associated with the CEM in Section 3.1. Finally, a peeling-type algorithm is constructed in Section 4 for implementing the regularized monotonicity method, and several numerical examples employing the CEM are presented.

1.1. Notational remarks. For brevity we denote the essential infima/suprema $\text{ess inf}_{x \in \Omega} f(x)$ and $\text{ess sup}_{x \in \Omega} f(x)$ by $\inf(f)$ and $\sup(f)$, respectively. Since the indefinite inclusions and the operators involved in the monotonicity method, require far more notation compared to the definite case, we constantly employ the symbols “+”/“-” to associate sets and operators to positive/negative inclusions. To avoid excessive repetition, we often use the notation \pm to indicate that a set inclusion or equation/inequality holds for both the “+” and “-” version of a set or operator. For example, $\mathcal{M}_\pm \subseteq \mathcal{M}_{\alpha_\pm}(T_\pm^{h,\delta})$ states that both set inclusions $\mathcal{M}_+ \subseteq \mathcal{M}_{\alpha_+}(T_+^{h,\delta})$ and $\mathcal{M}_- \subseteq \mathcal{M}_{\alpha_-}(T_-^{h,\delta})$ hold true.

2. Reconstruction of indefinite inclusions based on monotonicity. In this section the CM is formulated for an isotropic conductivity distribution. The essential monotonicity properties of the associated Neumann-to-Dirichlet map are revised to motivate the monotonicity method. Furthermore, in Section 2.2 the monotonicity method is formulated for the CM for reconstruction of irregular indefinite inclusions.

2.1. The continuum model. Let $\Omega \subset \mathbb{R}^d$ for $d \geq 2$ be an open, bounded, and simply connected domain with \mathcal{C}^∞ -regular boundary $\partial\Omega$. The CM is governed by the following elliptic boundary value problem

$$(2.1) \quad \nabla \cdot (\gamma \nabla u) = 0 \text{ in } \Omega, \quad \nu \cdot \gamma \nabla u = f \text{ on } \partial\Omega, \quad \int_{\partial\Omega} u \, ds = 0,$$

where ν is an outwards-pointing unit normal to $\partial\Omega$ and the real-valued conductivity distribution γ belongs to

$$(2.2) \quad L_+^\infty(\Omega) = \{w \in L^\infty(\Omega) : \inf(w) > 0\}.$$

The latter condition in (2.1) corresponds to a grounding of the electric potential. The Neumann boundary condition models the current density applied to the object at its boundary. According to standard elliptic theory, for any

$$f \in L_\diamond^2(\partial\Omega) = \{w \in L^2(\partial\Omega) : \langle w, 1 \rangle = 0\},$$

problem (2.1) has a unique weak solution u in

$$H_\diamond^1(\Omega) = \{w \in H^1(\Omega) : \langle w|_{\partial\Omega}, 1 \rangle = 0\}.$$

Here and in the remainder of the paper, $\langle \cdot, \cdot \rangle$ denotes the usual $L^2(\partial\Omega)$ -inner product, $w|_{\partial\Omega}$ denotes the trace of w on $\partial\Omega$, and $\mathbb{1} \equiv 1$ on $\partial\Omega$. This gives rise to a well-defined ND map

$$\Lambda(\gamma) : L_\diamond^2(\partial\Omega) \rightarrow L_\diamond^2(\partial\Omega), \quad f \mapsto u|_{\partial\Omega}.$$

The graph of the ND map corresponds to all possible pairs of applied current densities and measured boundary voltage, and as such $\Lambda(\gamma)$ models the (infinite precision) current-to-voltage datum for the CM. Note that $\Lambda(\gamma)$ belongs to $\mathcal{L}(L_\diamond^2(\partial\Omega))$, the space of linear and bounded operators on $L_\diamond^2(\partial\Omega)$, for each $\gamma \in L_+^\infty(\Omega)$. Moreover, $\Lambda(\gamma)$ is a compact and self-adjoint operator.

Although the forward map $\Lambda : L_+^\infty(\Omega) \rightarrow \mathcal{L}(L_\diamond^2(\partial\Omega))$ is non-linear, it is Fréchet differentiable on $L_+^\infty(\Omega)$ and the derivative is determined through the quadratic form (cf. [9, Appendix B])

$$(2.3) \quad \langle \Lambda'(\gamma)[\eta]f, f \rangle = - \int_\Omega \eta |\nabla u|^2 dx, \quad \eta \in L^\infty(\Omega)$$

where u is the solution to (2.1) for a conductivity distribution γ and Neumann condition f . The following proposition, along with (2.3), represents the essential monotonicity principles of Λ and Λ' which forms the basis for the monotonicity method.

PROPOSITION 2.1. *For each $f \in L_\diamond^2(\partial\Omega)$ and two arbitrary conductivities $\gamma, \tilde{\gamma} \in L_+^\infty(\Omega)$ it holds*

$$(2.4) \quad \int_\Omega \frac{\tilde{\gamma}}{\gamma} (\gamma - \tilde{\gamma}) |\nabla \tilde{u}|^2 dx \leq \langle (\Lambda(\tilde{\gamma}) - \Lambda(\gamma))f, f \rangle \leq \int_\Omega (\gamma - \tilde{\gamma}) |\nabla \tilde{u}|^2 dx$$

where \tilde{u} is the solution to (2.1) with conductivity $\tilde{\gamma}$ and Neumann condition f .

Proof. See, e.g., [15, Lemma 3.1]. \square

An immediate consequence of Proposition 2.1 is the simple monotonicity relation

$$(2.5) \quad \gamma \geq \tilde{\gamma} \text{ a.e. in } \Omega \quad \text{implies} \quad \Lambda(\tilde{\gamma}) \geq \Lambda(\gamma).$$

REMARK 1. *In (2.5) and in the remainder of the paper, an operator inequality of form $A \leq B \leq C$ for self-adjoint $A, B, C \in \mathcal{L}(L_\diamond^2(\partial\Omega))$ is understood in the sense of positive semi-definiteness, that is, $\langle (C - B)f, f \rangle \geq 0$ and $\langle (B - A)f, f \rangle \geq 0$ for all $f \in L_\diamond^2(\partial\Omega)$.*

2.2. The monotonicity method for irregular indefinite inclusions. In this section we review the general theory related to the monotonicity method for the CM based reconstruction of indefinite inclusions. Moreover, we introduce the notation that will be used later in Section 3.

Let us begin by defining the notion of an indefinite inclusion

DEFINITION 2.2 (Indefinite inclusion). *Consider a conductivity distribution of the form*

$$(2.6) \quad \gamma = \gamma_0 + \kappa_+ \chi_{D_+} - \kappa_- \chi_{D_-}$$

where $\gamma_0 \in L_+^\infty(\Omega)$ is piecewise real analytic, $\kappa_\pm \in L_+^\infty(\Omega)$, $\sup(\kappa_-) < \inf(\gamma_0)$, and $D_\pm \subseteq \Omega$ are open and disjoint. The set $D = D_+ \cup D_-$ is called an indefinite inclusion

with respect to the background conductivity γ_0 . The sets D_+ and D_- are called the positive part and negative part, respectively, of the inclusion.

REMARK 2. The condition $\sup(\kappa_-) < \inf(\gamma_0)$ is generally not required for the monotonicity method, and for homogeneous γ_0 (which is the default setting in [15]) this is automatically satisfied as we must have $\gamma \in L_+^\infty(\Omega)$. In the proof of Theorem 2.4 it will be evident that this additional assumption, along with $\kappa_\pm \in L_+^\infty(\Omega)$, greatly simplifies the monotonicity method. It furthermore implies the existence of an efficient algorithm that implements the monotonicity method; see Section 4.

The relation in (2.5) gives rise to a method of approximating the inclusion D by checking for various upper bounds C to D_+ and D_- ; see Theorem 2.4.(i). The reconstruction method was made precise in [15] by also considering the converse of (2.5). More precisely, counter examples to the monotonicity relation are proven using the theory of localized potentials when C is not an upper bound of D ; see [10] and Theorem 2.4.(ii). Below we formulate the results of [15] in the setting of Definition 2.2. Due to the assumption that the perturbations κ_\pm are essentially bounded away from zero, it is possible to state the result in a different way similar to what was done in [15, Examples 4.8 and 4.10], but for general L_+^∞ -perturbations. The assumptions in Definition 2.2 furthermore avoid the requirement that D_+ and D_- should be well-separated similar to what was considered in [15] when $\gamma - \gamma_0$ is assumed to be piecewise analytic.

Under the assumptions of Definition 2.2 there are positive constants β^L and β^U such that

$$(2.7) \quad \beta^L \leq \gamma_0 \leq \beta^U \text{ in } \Omega,$$

and there exists a large enough $\beta > 0$ which satisfies

$$(2.8) \quad \sup(\kappa_+) \leq \beta, \quad \sup(\kappa_-) \leq \frac{\beta}{1 + \beta} \beta^L.$$

A concept essential for characterizing the reconstructions from the monotonicity method is the *outer support* of a set.

DEFINITION 2.3 (Outer support). *The outer support X^\bullet of a subset $X \subseteq \bar{\Omega}$ is defined as*

$$X^\bullet = \bar{\Omega} \setminus \cup\{U \subseteq \mathbb{R}^d \setminus X \text{ open and connected} : U \cap \partial\Omega \neq \emptyset\},$$

and is the smallest closed set containing X and having connected complement in \mathbb{R}^d . If X has connected complement in \mathbb{R}^d then $X^\bullet = \bar{X}$.

We will make use of the notation $D_\pm^\bullet = (D_\pm)^\bullet$. The reason why Definition 2.3 uses connected complements in \mathbb{R}^d rather than in $\bar{\Omega}$ is the following. Any doubly connected subset $X \subseteq \bar{\Omega}$ satisfying $\partial\Omega \subset X$ has connected complement in $\bar{\Omega}$ but we do not necessarily have $\bar{X} = X^\bullet$. The convention that *connected complement* is understood as the complement in \mathbb{R}^d together with the assumption that Ω is simply connected takes care of this technicality. Hence, we can consistently state that any closed set $C \subseteq \bar{\Omega}$ with connected complement satisfies $C = C^\bullet$. Such sets will appear in most of the results for the monotonicity method. Consequently, we define the family of *admissible test inclusions* as

$$(2.9) \quad \mathcal{A} = \{C \subseteq \bar{\Omega} \text{ closed set} : \mathbb{R}^d \setminus C \text{ connected}\}.$$

The most important operators regarding the monotonicity method are

$$\begin{aligned}
 (2.10) \quad T_+(C) &= \Lambda(\gamma) - \Lambda(\gamma_0 + \beta\chi_C), \\
 T'_+(C) &= \Lambda(\gamma) - \Lambda(\gamma_0) - \beta\Lambda'(\gamma_0)\chi_C, \\
 T_-(C) &= \Lambda(\gamma_0 - \frac{\beta}{1+\beta}\beta^L\chi_C) - \Lambda(\gamma), \\
 T'_-(C) &= \Lambda(\gamma_0) - \beta^U\beta\Lambda'(\gamma_0)\chi_C - \Lambda(\gamma).
 \end{aligned}$$

Above notation for the parameter β is suppressed as it is only required to be large enough to satisfy (2.8)

Theorem 2.4 below characterizes the outer support D^\bullet in terms of the operators in (2.10). Although the result is very close to [15, Theorem 4.7 and 4.9], different assumptions imply that the equivalence condition is true for

1. a fixed β -parameter which is easy to pick,
2. a non-homogeneous background conductivity γ_0 ,
3. non-smooth $L_+^\infty(\Omega)$ perturbations.

Due to the listed differences, the proof is given for completion. In fact, the proof is also needed in Theorem 2.6 giving sufficient conditions for reconstructing D_+ and D_- independently.

THEOREM 2.4. *Assume that $\gamma \in L_+^\infty(\Omega)$ is as in Definition 2.2 and let $\beta > 0$ satisfy (2.8). Then the following statements hold true.*

(i) *For any measurable $C \subseteq \bar{\Omega}$,*

$$(2.11) \quad D_+ \subseteq C \quad \text{implies} \quad T_+(C) \geq 0 \quad \text{and} \quad T'_+(C) \geq 0,$$

$$(2.12) \quad D_- \subseteq C \quad \text{implies} \quad T_-(C) \geq 0 \quad \text{and} \quad T'_-(C) \geq 0.$$

(ii) *For any $C \in \mathcal{A}$,*

$$(2.13) \quad D^\bullet \subseteq C \quad \text{if and only if} \quad T_\pm(C) \geq 0 \quad \text{if and only if} \quad T'_\pm(C) \geq 0.$$

Proof of (i). The positive semi-definiteness of $T_+(C)$ and $T_-(C)$ in (2.11) and (2.12) is a direct consequence of the monotonicity relation (2.5) when $D_+ \subseteq C$ and $D_- \subseteq C$, respectively. For $D_+ \subseteq C$, let u_f denote the solution to (2.1) for Neumann condition $f \in L_\diamond^2(\partial\Omega)$ and conductivity γ_0 . By inserting $T'_+(C)$ into Proposition 2.1 and (2.3) and subsequently applying $\sup(\kappa_+) \leq \beta$ and $D_+ \subseteq C$ gives

$$\begin{aligned}
 -\langle T'_+(C)f, f \rangle &\leq \int_{\Omega} (\gamma - \gamma_0 - \beta\chi_C) |\nabla u_f|^2 dx \\
 &\leq \int_{\Omega} (\kappa_+ \chi_{D_+} - \beta\chi_C) |\nabla u_f|^2 dx \\
 &\leq \int_{\Omega} \beta(\chi_{D_+} - \chi_C) |\nabla u_f|^2 dx \leq 0
 \end{aligned}$$

for all $f \in L_\diamond^2(\partial\Omega)$. This demonstrates (2.11). Similarly $D_- \subseteq C$ with Proposition 2.1

yields

$$\begin{aligned}
\langle T'_-(C)f, f \rangle &\geq \int_{\Omega} \left[\frac{\gamma_0}{\gamma} (\gamma - \gamma_0) + \beta^U \beta \chi_C \right] |\nabla u_f|^2 dx \\
&\geq \int_{\Omega} \left[\gamma_0 \left(1 - \frac{\gamma_0}{\gamma_0 - \kappa_- \chi_{D_-}} \right) + \beta^U \beta \chi_C \right] |\nabla u_f|^2 dx \\
&= \int_{\Omega} \left[\beta^U \beta \chi_C - \frac{\gamma_0 \kappa_-}{\gamma_0 - \kappa_-} \chi_{D_-} \right] |\nabla u_f|^2 dx \\
&\geq \int_{\Omega} \beta^U \beta (\chi_C - \chi_{D_-}) |\nabla u_f|^2 dx \geq 0, \quad \forall f \in L^2_{\diamond}(\partial\Omega).
\end{aligned}$$

In the bottom inequality the bounds in (2.8) are applied through

$$(2.14) \quad \frac{\gamma_0 \kappa_-}{\gamma_0 - \kappa_-} \leq \frac{\beta^U \frac{\beta}{1+\beta} \beta^L}{\beta^L - \frac{\beta}{1+\beta} \beta^L} = \beta^U \beta.$$

Proof of (ii). The logical structure of this part of the proof can be outlined as

$$(2.15) \quad \begin{aligned} P &\Rightarrow P' \text{ and } P \Rightarrow P'', \\ \neg P &\Rightarrow \neg P' \text{ and } \neg P \Rightarrow \neg P'', \end{aligned}$$

where P, P', P'' are the conditions in the claimed equivalence relation in the same order from left to right as in the theorem statement.

Let $C \in \mathcal{A}$ be arbitrary. Then clearly $D \subset D^* \subseteq C$ implies the inequalities $T_{\pm}(C) \geq 0$ and $T'_{\pm}(C) \geq 0$ by (i). Subsequently it suffices to contradict either one of the $+/$ - inequalities if $D^* \not\subseteq C$. There are two possible cases:

- (a) $D_+^* \cap \partial D^* \not\subseteq C$,
- (b) $D_+^* \cap \partial D^* \subseteq C$ and $D_-^* \cap \partial D^* \not\subseteq C$.

Case (a): Since C and D^* have connected complement then we can pick a relatively open and connected set $U \subset \overline{\Omega}$ which intersects $\partial\Omega$ and has connected complement. The set U is chosen such that $U \cap C = \emptyset$, $U \cap D_- = \emptyset$, and such that $U \cap D_+$ contains an open ball B . This choice can be done as D_+ is open and C is closed; see Figure 1. The main structure of the proof is to construct potentials u where $|\nabla u|^2$ is large enough inside B and small enough outside U , such that the monotonicity principles in Proposition 2.1 contradict the inequalities $T_+(C) \geq 0$ and $T'_+(C) \geq 0$.

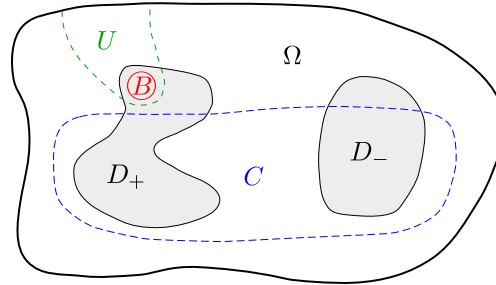


Fig. 1: Illustration of case (a) in the proof of Theorem 2.4.(ii).

We begin the argument by noting that $\gamma = \gamma_0 + \kappa_+$ on B , $\gamma \geq \gamma_0$ on U , and $(\overline{\Omega} \setminus U)^\bullet = \overline{\Omega} \setminus U$. Since γ_0 is piecewise analytic, then by [15, Theorem 3.6] there exist sequences of current densities $\{f_m^+\}_{m \in \mathbb{N}} \subset L_\diamond^2(\partial\Omega)$ and the corresponding potentials $\{u_m^{\gamma_0}\}_{m \in \mathbb{N}} \subset H_\diamond^1(\Omega)$, that solve (2.1) with conductivity γ_0 , such that we have

$$(2.16) \quad \lim_{m \rightarrow \infty} \int_B |\nabla u_m^{\gamma_0}|^2 dx = \infty, \quad \lim_{m \rightarrow \infty} \int_{\Omega \setminus U} |\nabla u_m^{\gamma_0}|^2 dx = 0.$$

Such solutions are commonly referred to as *localized potentials* [10]. Let $\hat{\gamma} = \frac{\gamma_0}{\gamma}(\gamma - \gamma_0) - \beta\chi_C$. By Proposition 2.1, (2.14), and (2.16), we get

$$\begin{aligned} & -\langle T'_+(C)f_m^+, f_m^+ \rangle \\ & \geq \int_{\Omega} \hat{\gamma} |\nabla u_m^{\gamma_0}|^2 dx \\ & = \int_B \frac{\gamma_0 \kappa_+}{\gamma_0 + \kappa_+} |\nabla u_m^{\gamma_0}|^2 dx + \int_{U \setminus B} \frac{\gamma_0 \kappa_+ \chi_{D_+}}{\gamma_0 + \kappa_+ \chi_{D_+}} |\nabla u_m^{\gamma_0}|^2 dx + \int_{\Omega \setminus U} \hat{\gamma} |\nabla u_m^{\gamma_0}|^2 dx \\ (2.17) \quad & \geq \frac{\beta^L \inf(\kappa_+)}{\beta^U + \beta} \int_B |\nabla u_m^{\gamma_0}|^2 dx - \beta(\beta^U + 1) \int_{\Omega \setminus U} |\nabla u_m^{\gamma_0}|^2 dx \rightarrow \infty \text{ for } m \rightarrow \infty. \end{aligned}$$

In other words, we have deduced the condition $T'_+(C) \not\geq 0$.

Since $C \subseteq \overline{\Omega} \setminus U$ then by [15, Lemma 3.7] there exists a sequence of localized potentials $\{u_m^{\tilde{\gamma}}\}_{m \in \mathbb{N}}$ and the corresponding current densities $\{g_m^+\}_{m \in \mathbb{N}}$ for the conductivity $\tilde{\gamma} = \gamma_0 + \beta\chi_C$. We denote $\hat{\gamma} = \frac{\gamma}{\tilde{\gamma}}(\gamma - \tilde{\gamma})$ and again apply Proposition 2.1 with the asymptotic properties of the localized potentials to obtain

$$\begin{aligned} & -\langle T_+(C)g_m^+, g_m^+ \rangle \\ & \geq \int_{\Omega} \hat{\gamma} |\nabla u_m^{\tilde{\gamma}}|^2 dx \\ & = \int_B \frac{\gamma_0 \kappa_+}{\gamma_0 + \kappa_+} |\nabla u_m^{\tilde{\gamma}}|^2 dx + \int_{U \setminus B} \frac{\gamma_0 \kappa_+ \chi_{D_+}}{\gamma_0 + \kappa_+ \chi_{D_+}} |\nabla u_m^{\tilde{\gamma}}|^2 dx + \int_{\Omega \setminus U} \hat{\gamma} |\nabla u_m^{\tilde{\gamma}}|^2 dx \\ (2.18) \quad & \geq \frac{\beta^L \inf(\kappa_+)}{\beta^U + \beta} \int_B |\nabla u_m^{\tilde{\gamma}}|^2 dx + \inf(\hat{\gamma}) \int_{\Omega \setminus U} |\nabla u_m^{\tilde{\gamma}}|^2 dx \rightarrow \infty \text{ for } m \rightarrow \infty. \end{aligned}$$

Notice that $\inf(\hat{\gamma}) > -\infty$ as $\gamma, \tilde{\gamma} \in L_+^\infty(\Omega)$. As a result of (2.18) we have $T_+(C) \not\geq 0$.

Case (b): In this case the roles of D_+ and D_- are switched when choosing the sets U and B , such that $\gamma = \gamma_0 - \kappa_-$ on B and $\gamma \leq \gamma_0$ on U .

Let $\hat{\gamma} = \gamma - \gamma_0 + \beta^U \beta \chi_C$. Using the localized potentials for γ_0 with current densities $\{f_m^-\}_{m \in \mathbb{N}}$ and the monotonicity relations in Proposition 2.1, we get

$$\begin{aligned} & \langle T'_-(C)f_m^-, f_m^- \rangle \\ & \leq \int_{\Omega} \hat{\gamma} |\nabla u_m^{\gamma_0}|^2 dx \\ & = - \int_B \kappa_- |\nabla u_m^{\gamma_0}|^2 dx - \int_{U \setminus B} \kappa_- \chi_{D_-} |\nabla u_m^{\gamma_0}|^2 dx + \int_{\Omega \setminus U} \hat{\gamma} |\nabla u_m^{\gamma_0}|^2 dx \\ (2.19) \quad & \leq -\inf(\kappa_-) \int_B |\nabla u_m^{\gamma_0}|^2 dx + \beta(\beta^U + 1) \int_{\Omega \setminus U} |\nabla u_m^{\gamma_0}|^2 dx \rightarrow -\infty \text{ for } m \rightarrow \infty, \end{aligned}$$

so $T'_-(C) \not\geq 0$.

Finally, let $\tilde{\gamma} = \gamma_0 - \frac{\beta}{1+\beta} \beta^L \chi_C$ and similar to case (a) we consider the localized potentials with respect to $\tilde{\gamma}$ with current densities $\{g_m^-\}_{m \in \mathbb{N}}$. From the monotonicity relations and properties of the localized potential we have

$$\begin{aligned}
 & \langle T_-(C)g_m^-, g_m^- \rangle \\
 & \leq \int_{\Omega} (\gamma - \tilde{\gamma}) |\nabla u_m^{\tilde{\gamma}}|^2 dx \\
 & = - \int_B \kappa_- |\nabla u_m^{\tilde{\gamma}}|^2 dx - \int_{U \setminus B} \kappa_- \chi_{D_-} |\nabla u_m^{\tilde{\gamma}}|^2 dx + \int_{\Omega \setminus U} (\gamma - \tilde{\gamma}) |\nabla u_m^{\tilde{\gamma}}|^2 dx \\
 (2.20) \quad & \leq -\inf(\kappa_-) \int_B |\nabla u_m^{\tilde{\gamma}}|^2 dx + \frac{1+\beta+\beta^L}{1+\beta} \beta \int_{\Omega \setminus U} |\nabla u_m^{\tilde{\gamma}}|^2 dx \rightarrow -\infty \text{ for } m \rightarrow \infty.
 \end{aligned}$$

Thus $T_-(C) \not\geq 0$, which concludes the proof. \square

To facilitate the formulation of a reconstruction algorithm based on Theorem 2.4.(ii) we define the following collections of test inclusions

$$\begin{aligned}
 \mathcal{M}_+ &= \{C \in \mathcal{A} : T_+(C) \geq 0\}, & \mathcal{M}'_+ &= \{C \in \mathcal{A} : T'_+(C) \geq 0\}, \\
 \mathcal{M}_- &= \{C \in \mathcal{A} : T_-(C) \geq 0\}, & \mathcal{M}'_- &= \{C \in \mathcal{A} : T'_-(C) \geq 0\}.
 \end{aligned}$$

Furthermore, we define $\mathcal{M} = \mathcal{M}_+ \cap \mathcal{M}_-$ and $\mathcal{M}' = \mathcal{M}'_+ \cap \mathcal{M}'_-$ as the collections of test inclusions that satisfy both inequalities.

COROLLARY 2.5. *Under the assumptions of Theorem 2.4 there holds*

$$(2.21) \quad D^\bullet = \cap \mathcal{M} = \cap \mathcal{M}'.$$

Proof. By Theorem 2.4.(ii) we have $\mathcal{M} = \mathcal{M}'$ and for any $C \in \mathcal{M}$ we have $D^\bullet \subseteq C$. Since $D^\bullet \in \mathcal{M}$ the claim follows. \square

By Corollary 2.5 the sets \mathcal{M} and \mathcal{M}' characterize the outer shape of D . Therefore it makes sense to consider \mathcal{M} and \mathcal{M}' as theoretical reconstructions output by the monotonicity method.

Under the additional assumption that all of ∂D_+^\bullet and ∂D_-^\bullet can be connected to $\partial\Omega$ by only traversing $\bar{\Omega} \setminus D$, then the monotonicity method can be split into two independent submethods; one that determines the positive part and another that determines the negative part.

THEOREM 2.6. *In addition to the assumptions of Theorem 2.4, assume that the outer boundaries of D_+ and D_- are well-separated, i.e. $\partial D_+^\bullet \cap \partial D_-^\bullet = \emptyset$.*

(i) *If $D_+ \cap D_-^\bullet = \emptyset$ then for any $C \in \mathcal{A}$ there holds*

$$(2.22) \quad D_+^\bullet \subseteq C \quad \text{if and only if} \quad T_+(C) \geq 0 \quad \text{if and only if} \quad T'_+(C) \geq 0.$$

In particular $D_+^\bullet = \cap \mathcal{M}_+ = \cap \mathcal{M}'_+$.

(ii) *If $D_- \cap D_+^\bullet = \emptyset$ then for any $C \in \mathcal{A}$ there holds*

$$(2.23) \quad D_-^\bullet \subseteq C \quad \text{if and only if} \quad T_-(C) \geq 0 \quad \text{if and only if} \quad T'_-(C) \geq 0.$$

In particular $D_-^\bullet = \cap \mathcal{M}_- = \cap \mathcal{M}'_-$.

Proof of (i): Clearly $D_+ \subset D_+^\bullet \subseteq C$ implies the inequalities $T_+(C) \geq 0$ and $T'_+(C) \geq 0$ in (2.22) by Theorem 2.4.(i).

If $D_+^\bullet \not\subseteq C$, then we can pick a relatively open set U and open ball B in the same way as in the proof of Theorem 2.4.(ii). The assumptions $D_+ \cap D_-^\bullet = \emptyset$ and

$\partial D_+^\bullet \cap \partial D_-^\bullet = \emptyset$ ensure that we can pick U such that $U \cap D_- = \emptyset$, and they are required to enable case (a) in the proof of Theorem 2.4.(ii). Hence, (2.17) and (2.18) contradict the inequalities in (2.22). The claim $D_+^\bullet = \cap \mathcal{M}_+ = \cap \mathcal{M}'_+$ is proved in the same way as Corollary 2.5.

Proof of (ii): The proof for D_- is similar to (i); when $D_-^\bullet \not\subseteq C$ then the inequalities in (2.23) are contradicted by (2.19) and (2.20). \square

REMARK 3. *If, for instance, the assumptions of Theorem 2.6.(i) hold, but $D_- \cap D_+^\bullet \neq \emptyset$, then D_-^\bullet and D_+^\bullet can be reconstructed but D_-^\bullet cannot. However, it is still possible to obtain information about D_- using the set $D_-^\bullet \setminus D_+^\bullet \subseteq D_-^\bullet$ which corresponds to the part of D_- that can be connected to $\partial\Omega$ without crossing D_+ .*

3. Regularizing the monotonicity method. In this section we formulate the regularized monotonicity method for indefinite inclusions. The presented construction is analogous to the definite case treated in [9].

In real-life measurements from EIT-devices there are two main sources of error:

1. *Modelling error* characterized by a parameter h , which states how closely related the actual measurements (or realistic electrode models) are to the CM.
2. *Noise error* controlled by a parameter $\delta > 0$. This error is caused by imperfections of the measurement device and it is not directly related to the model.

By symmetrizing if necessary, the noise error can be modelled as a self-adjoint operator $N^\delta \in \mathcal{L}(L_\diamond^2(\partial\Omega))$ which satisfies $\|N^\delta\|_{\mathcal{L}(L_\diamond^2(\partial\Omega))} \leq \delta$. Note that, in contrast to [9], here we have dropped the unnecessary assumption which requires N^δ to be compact.

To describe the modelling error we consider a family of compact and self-adjoint approximative operators $\{\Lambda_h(\gamma)\}_{h>0} \subset \mathcal{L}(L_\diamond^2(\Omega))$, such that the following estimate holds for each $\gamma \in L_+^\infty(\Omega)$,

$$(3.1) \quad \|\Lambda(\gamma) - \Lambda_h(\gamma)\|_{\mathcal{L}(L_\diamond^2(\partial\Omega))} \leq \omega(h) \|\gamma\|_{L^\infty(\Omega)}, \quad \lim_{h \rightarrow 0} \omega(h) = 0.$$

The measurements are now modelled with additive noise

$$(3.2) \quad \Lambda_h^\delta(\gamma) = \Lambda_h(\gamma) + N^\delta.$$

To adapt the monotonicity method with the approximative operators Λ_h and noisy measurements, we denote

$$\begin{aligned} T_+^h(C) &= \Lambda_h(\gamma) - \Lambda_h(\gamma_0 + \beta\chi_C), & T_-^h(C) &= \Lambda_h(\gamma_0 - \frac{\beta}{1+\beta}\beta^L\chi_C) - \Lambda_h(\gamma), \\ T_+^{h,\delta}(C) &= \Lambda_h^\delta(\gamma) - \Lambda_h(\gamma_0 + \beta\chi_C), & T_-^{h,\delta}(C) &= \Lambda_h(\gamma_0 - \frac{\beta}{1+\beta}\beta^L\chi_C) - \Lambda_h^\delta(\gamma). \end{aligned}$$

for any measurable $C \subseteq \overline{\Omega}$ (cf. Section 2.2). By (3.1) and [9, Lemma 1] the difference in infima of the spectra of $T_\pm^{h,\delta}$ and T_\pm satisfies the bound condition

$$|\inf \sigma(T_\pm^{h,\delta}(C)) - \inf \sigma(T_\pm(C))| \leq \omega(h) (\|\gamma_0\|_{L^\infty(\Omega)} + \|\gamma\|_{L^\infty(\Omega)} + \max\{\beta, \beta^L\}) + \delta$$

implying that

$$(3.3) \quad \lim_{h,\delta \rightarrow 0} \inf \sigma(T_\pm^{h,\delta}(C)) \rightarrow \inf \sigma(T_\pm(C)) \quad \text{uniformly in } C \subseteq \overline{\Omega}.$$

At this point we define the regularized reconstruction as $\cap \mathcal{M}_{\alpha_+, \alpha_-}(T_+^{h,\delta}, T_-^{h,\delta})$ where

$$\mathcal{M}_{\alpha_+, \alpha_-}(S_+, S_-) = \{C \in \mathcal{A} : S_\pm(C) + \alpha_\pm(C) \text{Id} \geq 0\}$$

and $\alpha_{\pm} : \mathcal{A} \rightarrow \mathbb{R}$ are regularization parameters which may depend on $C \in \mathcal{A}$ (see Remark 4), and $S_{\pm}(C) \in \mathcal{L}(L^2_{\diamond}(\partial\Omega))$ is self-adjoint for each measurable $C \subseteq \overline{\Omega}$. In addition, we denote $\mathcal{M}_{\alpha}(S) = \mathcal{M}_{\alpha,\alpha}(S, S)$. In particular, the reconstruction methods for the CM are included in this notation via $\mathcal{M} = \mathcal{M}_{0,0}(T_+, T_-)$ and $\mathcal{M}_{\pm} = \mathcal{M}_0(T_{\pm})$.

The following result establishes the convergence of the regularized monotonicity method, in the limit as the modelling error and noise error tend to zero.

THEOREM 3.1. *Suppose that the regularization parameters $\alpha_{\pm} = \alpha_{\pm}(h, \delta)[\cdot] : \mathcal{A} \rightarrow \mathbb{R}$ are bounded by*

$$\alpha_{\pm}^L(h, \delta) \leq \alpha_{\pm}(h, \delta)[C] \leq \alpha_{\pm}^U(h, \delta)$$

for all $C \in \mathcal{A}$ and $h, \delta > 0$, where α_{\pm}^L and α_{\pm}^U satisfy

$$(3.4) \quad \delta - \alpha_{\pm}^L(h, \delta) \leq \inf_{C \in \mathcal{M}} \inf \sigma(T_{\pm}^h(C)) \quad \text{and} \quad \lim_{h, \delta \rightarrow 0} \alpha_{\pm}^U(h, \delta) = 0.$$

Then for any $\lambda > 0$ there exists an $\epsilon_{\lambda} > 0$ such that

$$(3.5) \quad \mathcal{M} \subseteq \mathcal{M}_{\alpha_+(h, \delta), \alpha_-(h, \delta)}(T_+^{h, \delta}, T_-^{h, \delta}) \subseteq \mathcal{M}_{\lambda, \lambda}(T_+, T_-),$$

for all $h, \delta \in (0, \epsilon_{\lambda}]$.

Replacing \mathcal{M} by \mathcal{M}_{\pm} in (3.4) yields

$$(3.6) \quad \mathcal{M}_{\pm} \subseteq \mathcal{M}_{\alpha_{\pm}(h, \delta)}(T_{\pm}^{h, \delta}) \subseteq \mathcal{M}_{\lambda}(T_{\pm}),$$

for all $h, \delta \in (0, \epsilon_{\lambda}]$.

Proof. We only prove (3.5) since the adaptation of the proof for (3.6) is straightforward. First we prove the left-hand set inclusion in (3.5). Let $C \in \mathcal{M}$ be arbitrary, then

$$(3.7) \quad T_{\pm}^h(C) \geq \inf \sigma(T_{\pm}^h(C)) \text{Id} \geq (\delta - \alpha_{\pm}^L(h, \delta)) \text{Id}.$$

Since $\delta \text{Id} \geq \pm N^{\delta}$ then (3.7) implies

$$T_{\pm}^{h, \delta}(C) + \alpha_{\pm}(h, \delta)[C] \text{Id} = T_{\pm}^h(C) \pm N^{\delta} + \alpha_{\pm}(h, \delta)[C] \text{Id} \geq \delta \text{Id} \pm N^{\delta} \geq 0.$$

Thus $C \in \mathcal{M}_{\alpha_+(h, \delta), \alpha_-(h, \delta)}(T_+^{h, \delta}, T_-^{h, \delta})$ for all $h, \delta > 0$.

To prove the right-hand set inclusion in (3.5), let $\lambda_+ > 0$ and $\lambda_- > 0$ be arbitrary. The limit $\lim_{h, \delta \rightarrow 0} \alpha_{\pm}^U(h, \delta) = 0$ and (3.3) implies that there exist $\epsilon_{\lambda_+} > 0$ and $\epsilon_{\lambda_-} > 0$ such that

$$\alpha_{\pm}(h, \delta)[C] \leq \frac{\lambda_{\pm}}{2}, \quad \inf \sigma(T_{\pm}^{h, \delta}(C)) \leq \inf \sigma(T_{\pm}(C)) + \frac{\lambda_{\pm}}{2}$$

for all $h, \delta \in (0, \epsilon_{\lambda_{\pm}}]$ and $C \in \mathcal{A}$. Denote $\lambda = \max\{\lambda_+, \lambda_-\}$ and $\epsilon_{\lambda} = \min\{\epsilon_{\lambda_+}, \epsilon_{\lambda_-}\}$.

For any $C \in \mathcal{M}_{\alpha_+(h, \delta), \alpha_-(h, \delta)}(T_+^{h, \delta}, T_-^{h, \delta})$ we have

$$0 \leq \inf \sigma(T_{\pm}^{h, \delta}(C)) + \alpha_{\pm}(h, \delta)[C] \leq \inf \sigma(T_{\pm}(C)) + \lambda_{\pm} \leq \inf \sigma(T_{\pm}(C)) + \lambda,$$

which implies that $\mathcal{M}_{\alpha_+(h, \delta), \alpha_-(h, \delta)}(T_+^{h, \delta}, T_-^{h, \delta}) \subseteq \mathcal{M}_{\lambda, \lambda}(T_+, T_-)$ for all $h, \delta \in (0, \epsilon_{\lambda}]$. \square

Note that $0 < \lambda_{\pm} \leq \mu_{\pm}$ implies $\mathcal{M}_{\lambda_+, \lambda_-}(T_+, T_-) \subseteq \mathcal{M}_{\mu_+, \mu_-}(T_+, T_-)$, thus by monotonicity we have the set-theoretic limit

$$(3.8) \quad \lim_{\lambda \rightarrow 0} \mathcal{M}_{\lambda, \lambda}(T_+, T_-) = \bigcap_{\lambda > 0} \mathcal{M}_{\lambda, \lambda}(T_+, T_-) = \mathcal{M},$$

and likewise $\lim_{\lambda \rightarrow 0} \mathcal{M}_\lambda(T_\pm) = \mathcal{M}_\pm$. The sets $\mathcal{M}_{\alpha_+, \alpha_-}(T_+^{h, \delta}, T_-^{h, \delta})$ are not guaranteed to be monotone. However from (3.5) and the squeeze-principle we obtain the existence of a set-theoretic limit that coincides with \mathcal{M} .

COROLLARY 3.2. *Let the regularization parameters be as in Theorem 3.1. Then we have the set-theoretic limits*

$$\begin{aligned} \lim_{h, \delta \rightarrow 0} \mathcal{M}_{\alpha_+(h, \delta), \alpha_-(h, \delta)}(T_+^{h, \delta}, T_-^{h, \delta}) &= \mathcal{M} = \bigcap_{h, \delta > 0} \mathcal{M}_{\alpha_+(h, \delta), \alpha_-(h, \delta)}(T_+^{h, \delta}, T_-^{h, \delta}), \\ \lim_{h, \delta \rightarrow 0} \mathcal{M}_{\alpha_\pm(h, \delta)}(T_\pm^{h, \delta}) &= \mathcal{M}_\pm = \bigcap_{h, \delta > 0} \mathcal{M}_{\alpha_\pm(h, \delta)}(T_\pm^{h, \delta}). \end{aligned}$$

Proof. The proof is analogous to the proof in the definite case [9, Corollary 1]. \square
To conclude the section, we give a few remarks related to extensions of the regularized monotonicity method.

REMARK 4 (Related to Theorem 3.1 and Corollary 3.2).

1. **Regularized linear monotonicity method:** Define $(T'_\pm)^h$ and $(T'_\pm)^{h, \delta}$ as in Section 2.2 using the approximative models $\{\Lambda_h\}_{h > 0}$ and with noisy measurement $\Lambda_h^\delta(\gamma)$. Then Theorem 3.1 and Corollary 3.2 can be formulated using the linear monotonicity method by appropriately replacing \mathcal{M} , \mathcal{M}_\pm , T_\pm , T_+^h , and $T_\pm^{h, \delta}$ by \mathcal{M}' , \mathcal{M}'_\pm , T'_\pm , $(T'_\pm)^h$, and $(T'_\pm)^{h, \delta}$, respectively. The only additional assumption is that Λ_h is Fréchet differentiable with Λ'_h that for each $\gamma \in L_+^\infty(\Omega)$ and $\eta \in L^\infty(\Omega)$ satisfies the estimate

$$(3.9) \quad \|\Lambda'(\gamma)\eta - \Lambda'_h(\gamma)\eta\|_{\mathcal{L}(L_+^2(\partial\Omega))} \leq \omega(h)\|\gamma\|_{L^\infty(\Omega)}\|\eta\|_{L^\infty(\Omega)},$$

which gives the corresponding uniform convergence in (3.3) for $(T'_\pm)^{h, \delta}$ and T'_\pm .

2. **Regularization parameters:**

(i) Similar to [9] the regularization parameters can be chosen as

$$\alpha_\pm(h, \delta)[C] = \alpha_+^L(h, \delta) = \alpha_+^U(h, \delta),$$

i.e. independent of the set C (and the set of such admissible regularization parameters is non-empty). The reason for introducing the additional flexibility that α_\pm can depend on C , is because for a fixed $h, \delta > 0$ it turns out that varying the regularization depending on $|C|$ yields better numerical results. This was not observed in the definite case [9] since in those algorithms the numerical examples could be computed by checking monotonicity relations for balls of a fixed radius.

(ii) Assume that Λ_h satisfies the simple monotonicity relation (2.5), i.e.

$$(3.10) \quad \gamma \geq \tilde{\gamma} \quad \text{implies} \quad \Lambda_h(\tilde{\gamma}) \geq \Lambda_h(\gamma),$$

for all $\gamma, \tilde{\gamma} \in L_+^\infty(\Omega)$ and $h > 0$. By choosing $\beta > 0$ such that (2.8) is satisfied, then from Theorem 2.4.(ii) and the definition of \mathcal{M} , it holds

$$T_\pm^h(C) \geq T_\pm^h(D^\bullet) \geq 0, \quad C \in \mathcal{M}.$$

As a consequence, since $T_\pm^h(C)$ is compact and self-adjoint, it is sufficient to have $\alpha_\pm^L(h, \delta) \geq \delta$ in (3.4). The same conclusion holds for the regularization parameters in (3.6) if the assumptions of Theorem 2.6 are satisfied.

3. **Relation to the definite case:** From Theorem 3.1 it is clear that if we consider the reconstruction to be the intersection $\cap \mathcal{M}_{\alpha_+, \alpha_-}(T_+^{h, \delta}, T_-^{h, \delta})$, then we obtain a lower bound to the noise-free CM reconstruction,

$$\cap \mathcal{M}_{\alpha_+, \alpha_-}(T_+^{h, \delta}, T_-^{h, \delta}) \subseteq \cap \mathcal{M}.$$

This is in contrast to the definite case in [9] where an upper bound to D is obtained. Consider a definite case where $\gamma = \gamma_0 + \kappa_+ \chi_{D_+}$ and $\overline{D_+} \subseteq \Omega$ has a connected complement. Then we can guarantee a lower bound using the method for the indefinite case and an upper bound using the method for the definite case in [9] of D_+ , respectively. Moreover, the bounds converge from below and above, respectively, as both the noise and modelling error tend to zero.

4. **Including prior knowledge:** If a lower bound on the volume $t \leq |D^\bullet|$ of the inclusions is known, then we can consider

$$\mathcal{M}_{\alpha_+, \alpha_-}^t(T_+^{h, \delta}, T_-^{h, \delta}) \subseteq \mathcal{M}_{\alpha_+, \alpha_-}(T_+^{h, \delta}, T_-^{h, \delta})$$

as the subset for which $|C| \geq t$. The proof of Theorem 3.1 directly adapts to such prior information, where similarly we have $\mathcal{M}_{\lambda, \alpha_-}^t(T_+, T_-)$ on the right-hand side in (3.5). Then we obtain tighter reconstructions the closer the bound is to $|D^\bullet|$, i.e. for $t_1 \leq t_2 \leq |D^\bullet|$,

$$\cap \mathcal{M}_{\alpha_+, \alpha_-}^{t_1}(T_+^{h, \delta}, T_-^{h, \delta}) \subseteq \cap \mathcal{M}_{\alpha_+, \alpha_-}^{t_2}(T_+^{h, \delta}, T_-^{h, \delta}) \subseteq \cap \mathcal{M}.$$

5. **Operator estimates:** In the estimate (3.1) the dependence on γ only through $\|\gamma\|_{L^\infty(\Omega)}$ is needed for the uniform convergence in (3.3). Thus, the estimate (3.1) can be relaxed, by having $\omega(h)q(\|\gamma\|_{L^\infty(\Omega)})$ on the right-hand side with $q : [0, \infty) \rightarrow [0, \infty)$ a non-decreasing function. Furthermore, the estimate is also only required to hold for γ in Definition 2.2, $\gamma_0 + \beta \chi_C$, and $\gamma_0 - \frac{\beta}{1+\beta} \beta^L \chi_C$ with $C \in \mathcal{A}$.

6. **Formulation with pseudospectra:** The inequality $T_\pm^{h, \delta}(C) + \alpha_\pm(C) \text{Id} \geq 0$ is related to the so called δ -pseudospectrum of $T_\pm^h(C)$ by

$$\sigma(T_\pm^{h, \delta}(C) + \alpha_\pm(C) \text{Id}) \subseteq \alpha_\pm(C) + \sigma_\delta(T_\pm^h(C)).$$

Since $\cap_{\delta > 0} \sigma_\delta(T_\pm^h(C)) = \sigma(T_\pm^h(C))$ [33, Theorem 4.3], one can partly understand the limit in Corollary 3.2 in the sense of pseudospectra. More discussions on this topic are left for future studies.

Before discussing implementation details and numerical examples, we give an example of an approximate family $\{\Lambda_h\}_{h>0}$ constructed in terms of the CEM thus justifying the use of that model within the regularized monotonicity method.

3.1. Example – The Complete Electrode Model. In this section we show that the convergence results from Theorem 3.1 and Corollary 3.2 apply to the CEM, in fact we show that the very recent generalization, *Smoothed Complete Electrode Model* (SCEM) [20], satisfies the required bounds in (3.1) and (3.9).

To model the position of physical surface electrodes consider k open connected subsets $E_j \subseteq \partial\Omega$, $j = 1, 2, \dots, k$, where $\{\overline{E_j}\}_{j=1}^k$ are mutually disjoint. Furthermore, let the real-valued $\zeta \in L^\infty(\partial\Omega)$ model the contact impedance satisfying

$$(3.11) \quad \zeta \geq 0, \quad \zeta = 0 \text{ on } \partial\Omega \setminus \cup_{j=1}^k \overline{E_j}, \quad \zeta_j = \int_{E_j} \zeta \, dS > 0, \quad j = 1, 2, \dots, k.$$

The SCEM is defined as

$$(3.12) \quad \nabla \cdot (\gamma \nabla v) = 0, \quad \text{in } \Omega,$$

$$(3.13) \quad \nu \cdot \gamma \nabla v = \zeta(V - v), \quad \text{on } \partial\Omega,$$

$$(3.14) \quad \int_{E_j} \nu \cdot \gamma \nabla v \, dS = I_j, \quad j = 1, 2, \dots, k.$$

Here $v \in H^1(\Omega)$ is the interior electric potential, and the electrode voltages V and input net current pattern I belong to the hyperplane

$$\mathbb{R}_\diamond^k = \left\{ W \in \mathbb{R}^k : \sum_{j=1}^k W_j = 0 \right\}.$$

Note two things: firstly, for notational simplicity, we use the identification of $V \in \mathbb{R}_\diamond^k$ with the piecewise constant function GV , for G defined as

$$GW = \sum_{j=1}^k \chi_j W_j, \quad W \in \mathbb{R}^k,$$

where χ_j is the characteristic function on E_j . Secondly, if we use the specific choice $\zeta = G\tilde{z}$ with $\tilde{z}_j = z_j^{-1} > 0$ for $j = 1, 2, \dots, k$, then (3.12)–(3.14) states the usual CEM with constant contact impedance z_j on electrode E_j .

The PDE problem (3.12)–(3.14) admits a unique solution pair $(v, V) \in H^1(\Omega) \oplus \mathbb{R}_\diamond^k$ which follows from a standard application of the Lax-Milgram theorem [20, Theorem 2.2]. The advantage of the SCEM formulation, from a numerical point of view, is that the regularity of v depends directly on the regularity of ζ which affects the convergence rate of a finite element approximation [20, Theorem 2.5].

Similar to the standard CEM a linear, bounded, and self-adjoint current-to-voltage measurement map can be defined as

$$(3.15) \quad R(\gamma) : \mathbb{R}_\diamond^k \rightarrow \mathbb{R}_\diamond^k, \quad I \mapsto V.$$

In order to apply the theory from Theorem 3.1, Corollary 3.2, and Remark 4 we need to construct Λ_h -operators that relate the measurement map $R(\gamma)$ to the ND map $\Lambda(\gamma)$, such that Λ_h is Fréchet differentiable and satisfies the estimates (3.1) and (3.9); for the Fréchet differentiability and monotonicity properties of the SCEM see Appendix A. To this end we prove estimates of the type [19] and [9, Theorem 2 and 3] for the SCEM in Theorem 3.3. Before stating the theorem, we introduce the operators used to define the approximation to the CM.

Define mutually disjoint, connected, and open *artificial extended electrodes* $\{E_j^+\}_{j=1}^k$ which, together with the physical electrodes $\{E_j\}_{j=1}^k$, satisfy

$$(3.16) \quad E_j \subseteq E_j^+ \subseteq \partial\Omega, \quad \bigcup_{j=1}^k \overline{E_j^+} = \partial\Omega, \quad \min_{j=1, \dots, k} \frac{|E_j|}{|E_j^+|} \geq c,$$

for $c > 0$ independent of the set of electrodes. The latter condition in (3.16) implies a connection between the electrode size and the number of electrodes; if we let the electrode size tend to zero then the number of electrodes must grow in order to densely cover the boundary by small electrodes.

Let $L : L^2(\partial\Omega) \rightarrow L_\diamond^2(\partial\Omega)$ be an orthogonal projection and define $Q : \mathbb{R}^k \rightarrow L^2(\partial\Omega)$ and its adjoint Q^* by

$$QW = \sum_{j=1}^k W_j \chi_j^+, \quad (Q^*f)_j = \int_{E_j^+} f \, dS$$

where χ_j^+ is the characteristic function on E_j^+ . Finally, consider $P : L^2(\partial\Omega) \rightarrow \mathbb{R}^k$ as

$$(Pf)_j = \zeta_j^{-1} \int_{E_j} f \zeta \, dS, \quad j = 1, 2, \dots, k.$$

If we define a measure $d\mu_\zeta = \zeta \, dS$ then $(Pf)_j = \int_{E_j} f \, d\mu_\zeta$, and thus generalizes the P -operator from [9] to the SCEM.

We can now state the estimates for the SCEM.

THEOREM 3.3. *Denote the maximal extended electrode diameter by*

$$h = \max_j \text{diam}(E_j^+).$$

Assume that the extended electrodes are sufficiently regular that the Poincaré inequality-type estimate

$$(3.17) \quad \|(\text{Id} - QP)f\|_{L^2(\partial\Omega)} \leq Ch \inf_{c \in \mathbb{R}} \|f + c\|_{H^1(\partial\Omega)},$$

holds for all $f \in H^1(\partial\Omega)$ with a constant $C > 0$ independent of h . Then for each $\eta \in L^\infty(\Omega)$ and $\gamma \geq \beta^L/(1 + \beta)$ as in Definition 2.2, with $\overline{D}, \text{supp } \eta \subset \Omega$, we have

$$(3.18) \quad \|\Lambda(\gamma) - LQ(R(\gamma) - Z)Q^*\|_{\mathcal{L}(L_\diamond^2(\partial\Omega))} \leq C_\beta h \|\gamma\|_{L^\infty(\Omega)},$$

$$(3.19) \quad \|\Lambda'(\gamma)\eta - LQ(R'(\gamma)\eta)Q^*\|_{\mathcal{L}(L_\diamond^2(\partial\Omega))} \leq C_\beta h \|\gamma\|_{L^\infty(\Omega)} \|\eta\|_{L^\infty(\Omega)},$$

where the constant $C_\beta > 0$ is independent of h , γ , and η . Here $Z \in \mathbb{R}^{k \times k}$ is the diagonal matrix with non-zero entries $Z_{j,j} = \zeta_j^{-1}$.

Proof. The proof is inspired by the proof of [19, Theorem 4.1]. We denote by u the CM solution to (2.1) with Neumann condition $f \in L_\diamond^2(\partial\Omega)$ and by (v, V) the SCEM solution to (3.12)–(3.14) with current pattern Q^*f . Similar to [9] we denote u' and (v', V') as the solutions to the PDE-problems related to the Fréchet derivatives, with $u'|_{\partial\Omega} = \Lambda'(\gamma)[\eta]f$ and $V' = R'(\gamma)[\eta]Q^*f$.

By noting that $V = PV$ and applying the boundary conditions (3.13) and (3.14), then

$$\begin{aligned} Q(R(\gamma) - Z)Q^*f &= QPV - QZQ^*f \\ &= \sum_{j=1}^k \frac{\chi_j^+}{\zeta_j} \int_{E_j} \zeta V_j \, dS - QZQ^*f \\ &= \sum_{j=1}^k \frac{\chi_j^+}{\zeta_j} \left(\int_{E_j} \zeta v \, dS + \int_{E_j} \nu \cdot \gamma \nabla v \, dS \right) - QZQ^*f \\ (3.20) \quad &= QP(v|_{\partial\Omega}). \end{aligned}$$

Here it should be mentioned that the latter condition in (3.16) implies that QZQ^* is uniformly bounded with respect to h . Now inserting (3.20) into (3.18) and using the fact $\|L\|_{\mathcal{L}(L^2(\partial\Omega))} = 1$,

$$\begin{aligned} \|(\Lambda(\gamma) - LQ(R(\gamma) - Z)Q^*)f\|_{L^2(\partial\Omega)} &= \|u - LQPv\|_{L^2(\partial\Omega)} \\ (3.21) \quad &\leq \|u - Lv\|_{L^2(\partial\Omega)} + \|(\text{Id} - QP)v\|_{L^2(\partial\Omega)}. \end{aligned}$$

To estimate the terms in (3.21) we will need an L^2 -estimate on $\nu \cdot \gamma \nabla v$. From (3.13), the triangle inequality, the trace theorem, and the inequality $2ab \leq a^2 + b^2$ we clearly have

$$\begin{aligned} \|\nu \cdot \gamma \nabla v\|_{L^2(\partial\Omega)} &\leq C\|V - v\|_{L^2(\partial\Omega)} \\ &\leq C(\|V - c\|_{L^2(\partial\Omega)}^2 + \|v - c\|_{H^1(\Omega)}^2)^{1/2} \\ &\leq C(\|V - c\mathbf{1}\|_2^2 + \|v - c\|_{H^1(\Omega)}^2)^{1/2}, \end{aligned}$$

for all $c \in \mathbb{R}$, where $\mathbf{1} = (1, 1, \dots, 1) \in \mathbb{R}^k$. The operator Q^* is bounded independent of h by $\|Q^*\|_{\mathcal{L}(L^2(\partial\Omega), \mathbb{R}^k)}^2 \leq \max_j |E_j^+| \leq |\partial\Omega|$. Hence, due to the Lax-Milgram bound [20, Theorem 2.2] then $\nu \cdot \gamma \nabla v$ is bounded in $L^2(\partial\Omega)$ by f ,

$$\begin{aligned} \|\nu \cdot \gamma \nabla v\|_{L^2(\partial\Omega)} &\leq C \inf_{c \in \mathbb{R}} (\|V - c\mathbf{1}\|_2^2 + \|v - c\|_{H^1(\Omega)}^2)^{1/2} \\ &\leq C\|Q^*f\|_2 \\ (3.22) \quad &\leq C\|f\|_{L^2(\partial\Omega)}. \end{aligned}$$

The second term on the right-hand side in (3.21) is handled by the estimate (3.17), the trace theorem for quotient spaces [18], continuous dependence of v on the Neumann condition, and (3.22)

$$\begin{aligned} \|(\text{Id} - QP)v\|_{L^2(\partial\Omega)} &\leq Ch \inf_{c \in \mathbb{R}} \|v + c\|_{H^1(\partial\Omega)} \\ &\leq Ch \inf_{c \in \mathbb{R}} \|v + c\|_{H^{3/2}(\Omega)} \\ &\leq Ch\|\gamma\|_{L^\infty(\Omega)}\|\nu \cdot \gamma \nabla v\|_{L^2(\partial\Omega)} \\ (3.23) \quad &\leq Ch\|\gamma\|_{L^\infty(\Omega)}\|f\|_{L^2(\partial\Omega)}. \end{aligned}$$

Here the constant C depends on $\beta > 0$ satisfying $\gamma \geq \beta^L - \frac{\beta}{1+\beta}\beta^L = \frac{\beta^L}{1+\beta}$ to give uniform coercivity of the bilinear form in (A.1) with respect to γ ; this dependence will also be present in the following estimate. Since $\text{supp}(\nu \cdot \gamma \nabla v) \subseteq \bigcup_{j=1}^k \overline{E_j}$ then $Q^*f = Q^*(\nu \cdot \gamma \nabla v)$, so by continuous dependence on the Neumann condition,

$$\begin{aligned} \|u - Lv\|_{L^2(\partial\Omega)} &\leq C\|\gamma\|_{L^\infty(\Omega)}\|\nu \cdot \gamma \nabla(u - v)\|_{H^{-1}(\partial\Omega)} \\ &= C\|\gamma\|_{L^\infty(\Omega)}\|f - \nu \cdot \gamma \nabla v\|_{H^{-1}(\partial\Omega)} \\ &\leq C\|\gamma\|_{L^\infty(\Omega)} (\|(\text{Id} - QP)^*f\|_{H^{-1}(\partial\Omega)} + \|\nu \cdot \gamma \nabla v - (QP)^*f\|_{H^{-1}(\partial\Omega)}) \\ (3.24) \quad &= C\|\gamma\|_{L^\infty(\Omega)} (\|(\text{Id} - QP)^*f\|_{H^{-1}(\partial\Omega)} + \|(\text{Id} - QP)^*(\nu \cdot \gamma \nabla v)\|_{H^{-1}(\partial\Omega)}), \end{aligned}$$

where $(\text{Id} - QP)^*$ is the $L^2(\partial\Omega)$ -adjoint. For any $g \in L^2(\partial\Omega)$ then $(\text{Id} - QP)^*$ has the

following bound due to (3.17),

$$\begin{aligned}
\|(\text{Id} - QP)^*g\|_{H^{-1}(\partial\Omega)} &= \sup_{\|\phi\|_{H^1(\partial\Omega)}=1} |\langle (\text{Id} - QP)^*g, \phi \rangle| \\
&= \sup_{\|\phi\|_{H^1(\partial\Omega)}=1} |\langle g, (\text{Id} - QP)\phi \rangle| \\
&\leq \|g\|_{L^2(\partial\Omega)} \sup_{\|\phi\|_{H^1(\partial\Omega)}=1} \|(\text{Id} - QP)\phi\|_{L^2(\partial\Omega)} \\
(3.25) \quad &\leq Ch\|g\|_{L^2(\partial\Omega)}.
\end{aligned}$$

Inserting (3.25) and (3.22) into (3.24) gives

$$\|u - Lv\|_{L^2(\partial\Omega)} \leq Ch\|\gamma\|_{L^\infty(\Omega)}\|f\|_{L^2(\partial\Omega)},$$

which together with (3.21) and (3.23) concludes the proof of the estimate (3.18).

From similar calculations to (3.20) we obtain

$$(3.26) \quad QR'(\gamma)[\eta]Q^*f = QPV' = QP(v'|_{\partial\Omega}).$$

Thus, applying the trace theorem and that $\|L\|_{\mathcal{L}(L^2(\partial\Omega))} = 1$, gives the estimate

$$(3.27) \quad \|(\Lambda'(\gamma)\eta - LQR'(\gamma)[\eta]Q^*)f\|_{L^2(\partial\Omega)} \leq C\|u' - Lv'\|_{H^1(\Omega)} + \|(\text{Id} - QP)v'\|_{L^2(\partial\Omega)}.$$

Proving that both terms on the right-hand side of (3.27) are bounded by

$$Ch\|\gamma\|_{L^\infty(\Omega)}\|\eta\|_{L^\infty(\Omega)}\|f\|_{L^2(\partial\Omega)}$$

is now analogous to the proof of [9, Theorem 3]. \square

The approximative operators for the SCEM are now defined as

$$(3.28) \quad \Lambda_h(\gamma) = LQ(R(\gamma) - Z)Q^*,$$

$$(3.29) \quad \Lambda'_h(\gamma)\eta = LQ(R'(\gamma)\eta)Q^*.$$

Thus, the convergence result in Corollary 3.2 applies to the SCEM in the limit as the boundary is covered by sufficiently small and densely placed electrodes.

By inserting (3.28) into T_\pm^h yields

$$\begin{aligned}
T_+^h(C) &= LQ(R(\gamma) - R(\gamma_0 + \beta\chi_C))Q^*, \\
T_-^h(C) &= LQ(R(\gamma_0 - \frac{\beta}{1+\beta}\beta^L\chi_C) - R(\gamma))Q^*.
\end{aligned}$$

Since it holds for any linear operator $A : \mathbb{R}_\circ^k \rightarrow \mathbb{R}_\circ^k$ that $LQAQ^* \geq 0$ if and only if $A \geq 0$ (e.g. [9, Proposition 4]), it follows that the monotonicity tests for the reconstruction $\mathcal{M}_{\alpha_+, \alpha_-}(T_+^{h,\delta}, T_-^{h,\delta})$ can be evaluated directly from the measurement maps alone. Thus, the SCEM variant of the monotonicity method is simply a replacement of the ND map with the SCEM measurement map. Similarly can be done for the linear version of the monotonicity method.

4. Implementation details and numerical examples. In this section we outline a peeling-type algorithm for implementing the regularized monotonicity method for indefinite inclusions. The main idea is to initialize with a set $C \in \mathcal{A}$, represented in a pixel discretization, that contains D . Afterwards, we successively remove pixels from the boundary of the discretization of C if the new smaller set yields positive

semi-definiteness in the monotonicity tests. That is, we peel layers from C while maintaining that $C \in \mathcal{A}$ and yields positive semi-definiteness in the monotonicity tests.

We clearly have

$$(4.1) \quad \mathcal{M}_{\alpha_+^L, \alpha_-^L}(T_+^{h,\delta}, T_-^{h,\delta}) \subseteq \mathcal{M}_{\alpha_+, \alpha_-}(T_+^{h,\delta}, T_-^{h,\delta}) \subseteq \mathcal{M}_{\alpha_+^U, \alpha_-^U}(T_+^{h,\delta}, T_-^{h,\delta}).$$

Thus, if the presented algorithm is meaningful for regularization parameters independent of $C \in \mathcal{A}$, i.e. α_{\pm}^L and α_{\pm}^U , then the squeeze-principle and Corollary 3.2 imply that the algorithm will still converge in the limit as $h, \delta \rightarrow 0$ when using regularization parameters depending on C .

To relate the algorithm to the theory presented in Section 3 we assume that Λ_h satisfies the simple monotonicity relation (3.10), which is true for the SCEM example in Section 3.1 by Proposition A.1. Definition 2.2 implies that a single fixed β -value can be used for the monotonicity tests for any $C \in \mathcal{A}$, i.e. we have that $\gamma_0 - \frac{\beta}{1+\beta} \beta^L \chi_C$ is in $L_+^\infty(\Omega)$ for any $C \in \mathcal{A}$. Combined with the monotonicity relation, then

$$\begin{aligned} \mathcal{M}_{\alpha_+^L, \alpha_-^L}(T_+^{h,\delta}, T_-^{h,\delta}) \ni C_1 \subseteq C_2 \in \mathcal{A} &\quad \text{implies} \quad C_2 \in \mathcal{M}_{\alpha_+^L, \alpha_-^L}(T_+^{h,\delta}, T_-^{h,\delta}), \\ \mathcal{M}_{\alpha_+^U, \alpha_-^U}(T_+^{h,\delta}, T_-^{h,\delta}) \ni C_1 \subseteq C_2 \in \mathcal{A} &\quad \text{implies} \quad C_2 \in \mathcal{M}_{\alpha_+^U, \alpha_-^U}(T_+^{h,\delta}, T_-^{h,\delta}). \end{aligned}$$

Hence, it is meaningful to initialize with a large set $C \in \mathcal{A}$ and shrink it as long as it yields positive semi-definiteness in the monotonicity relations.

REMARK 5. Note that without the assumption $\sup(\kappa_-) < \inf(\gamma_0)$ in Definition 2.2, which allows the use of a fixed $\beta > 0$, there is the possibility that β can only be chosen large enough for the monotonicity relations when C is a slight upper bound to D ; see Figure 2. In that case there is no obvious efficient algorithm for the reconstruction, and one must check monotonicity relations for all $C \in \mathcal{A}$.

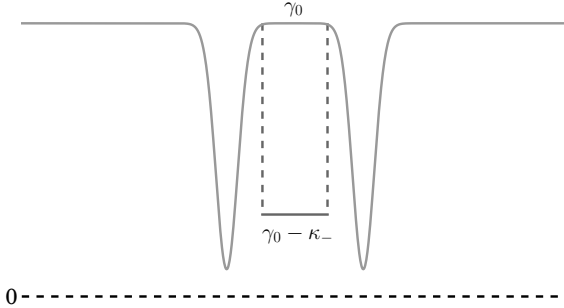


Fig. 2: Profile of a conductivity distribution γ which does not satisfy the assumption $\sup(\kappa_-) < \inf(\gamma_0)$.

To describe the implementation details we consider a regular pixel discretization $\{p_j\}_{j \in \mathcal{X}}$ of $\overline{\Omega}$ (voxel discretization in dimension three), where \mathcal{X} is a finite index set and $p_j \subseteq \overline{\Omega}$ with pixel size $|p_j| = \rho > 0$. Thus, a set $C \in \mathcal{A}$ is represented as $C_{\mathcal{J}} = \cup_{j \in \mathcal{J}} p_j$ where $\mathcal{J} \subseteq \mathcal{X}$ denotes an index set with the pixel indices. To handle the bookkeeping involved in the algorithm, for a given reconstruction candidate $C_{\mathcal{J}}$, we consider the three index sets $\mathcal{J}, \mathcal{I}, \mathcal{Y} \subseteq \mathcal{X}$ defined as follows:

- \mathcal{J} : indices of pixels in the set $C_{\mathcal{J}}$.
- \mathcal{I} : indices of boundary pixels of $C_{\mathcal{J}}$ that are yet to be tested if they can be removed.
- \mathcal{Y} : indices of pixels that have already been tested.

Hence, the algorithm can be described by the pseudocode in Algorithm 1, where *neighbour pixels* refer to the closest four neighbours (NWSE) in two dimensions and the closest six neighbours in three dimensions, i.e. not diagonal pixels.

Algorithm 1 Monotonicity-based reconstruction of indefinite inclusions

```

# initialize
1:  $\mathcal{J} := \{j \in \mathcal{X} : j \text{ is a pixel index from the initial given } C_{\mathcal{J}}\}$ 
2:  $\mathcal{I} := \{j \in \mathcal{J} : j \text{ is a boundary pixel of } C_{\mathcal{J}}\}$ 
3:  $\mathcal{Y} := \mathcal{X} \setminus \mathcal{J}$ 
4: for  $i \in \mathcal{I}$  do
    # test if pixel  $i$  can be removed
    5:  $\tilde{\mathcal{J}} := \mathcal{J} \setminus \{i\}$ ,  $\mathcal{I} := \mathcal{I} \setminus \{i\}$ ,  $\mathcal{Y} := \mathcal{Y} \cup \{i\}$ 
    6: Perform regularized monotonicity tests for  $C_{\tilde{\mathcal{J}}}$ 
    7: if monotonicity tests are positive semi-definite then
        # remove pixel  $i$  from reconstruction
        8:  $\mathcal{J} := \tilde{\mathcal{J}}$ 
        # add new boundary pixels of  $C_{\mathcal{J}}$  to be tested
        9:  $\mathcal{I} := \mathcal{I} \cup \{m \in \mathcal{J} \setminus \mathcal{Y} : m \text{ neighbour pixel to } i\}$ 
    10: end if
11: end for
    # the algorithm terminates when  $\mathcal{I} = \emptyset$ 
12: Return reconstruction  $C_{\mathcal{J}}$ 

```

Arguably, the algorithm for the indefinite case is more complicated than for the definite case in [9] since we are required to keep track of the inclusion boundary in each step. For the computational complexity, however, the methods are equivalent. Depending on the size of D the indefinite case may actually be significantly faster as the algorithm does not have to perform monotonicity tests for all the pixels in the domain, unlike the definite case. Furthermore, the algorithm can be initialized by attempting to remove all the boundary pixels of $C_{\mathcal{J}}$ simultaneously, and transition to removing single pixels when it fails to remove the whole boundary.

For the numerical examples we will use the linear version of the monotonicity method for the standard CEM with $z = 10^{-2}$ on all electrodes; numerical tests with the definite case suggests that the linear and nonlinear methods are equally noise robust [7]. Furthermore, we will only give reconstructions based on \mathcal{M}_+ and \mathcal{M}_- such that only a single regularization parameter is required. As mentioned in Remark 4 it is sufficient to have $\alpha_{\pm}^L \geq \delta$. As the regularization parameter for a fixed noise level $\delta > 0$ we use

$$(4.2) \quad \alpha(C) = \frac{\alpha_0}{|C|},$$

where $\alpha_0 \geq |\Omega|\delta$ is to be tuned. We assume that at least one pixel will be in the reconstruction such that $0 < \rho \leq |C| \leq |\Omega|$ for the considered test inclusions, thus satisfying (3.4). The choice (4.2) implies that smaller sets $C \in \mathcal{A}$ are regularized more in the monotonicity tests; this choice is not known to be optimal, but it did

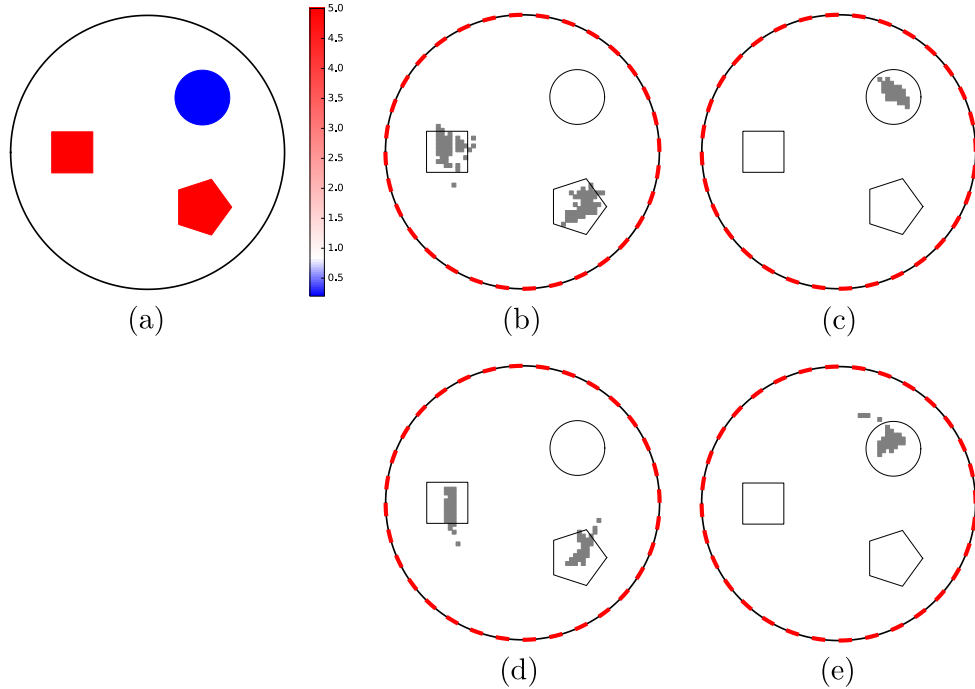


Fig. 3: (a) Two dimensional numerical phantom with positive part D_+ (square and pentagon) and negative part D_- (ball). (b) Reconstruction of D_+ from noiseless datum with $\alpha_0 = 6.56 \times 10^{-4}$. (c) Reconstruction of D_- from noiseless datum with $\alpha_0 = 2.36 \times 10^{-3}$. (d) Reconstruction of D_+ with 0.5% noise and $\alpha_0 = 5.00 \times 10^{-3}$. (e) Reconstruction of D_- with 0.5% noise and $\alpha_0 = 2.30 \times 10^{-3}$.

improve upon the reconstructions compared to using a uniform parameter. We also hypothesize that the distance of C to the boundary has an important role in an optimal choice of regularization [8]. However, we leave a detailed analysis regarding regularization parameter choices for future studies.

In the numerical examples we use the orthonormal set of current patterns $\mathbf{I} = [I^{(1)}, I^{(2)}, \dots, I^{(k-1)}]$ defined by

$$(4.3) \quad I_j^{(m)} = \begin{cases} \sqrt{\frac{1}{m(m+1)}} & j = 1, 2, \dots, m, \\ -\sqrt{\frac{m}{m+1}} & j = m+1, \\ 0 & j = m+2, m+3, \dots, k. \end{cases}$$

Note that (4.3) is the Gram–Schmidt orthonormalization of the standard basis $\{e^{(1)} - e^{(m+1)}\}_{m=1}^{k-1}$ for \mathbb{R}_\diamond^k .

In each example we simulate $V^{(m)} = R(\gamma)I^{(m)}$, and collect the output as

$$\mathbf{V} = [V^{(1)}, V^{(2)}, \dots, V^{(k-1)}].$$

To simulate noise, define the $k \times k$ matrix \mathbf{Y} with $\mathbf{Y}_{i,j}$ drawn from a normal $\mathcal{N}(0, 1)$ -distribution. Now we consider the perturbed measurements

$$\tilde{\mathbf{V}} = \mathbf{H}(\text{Id}_k + \mathbf{Y})\mathbf{V},$$

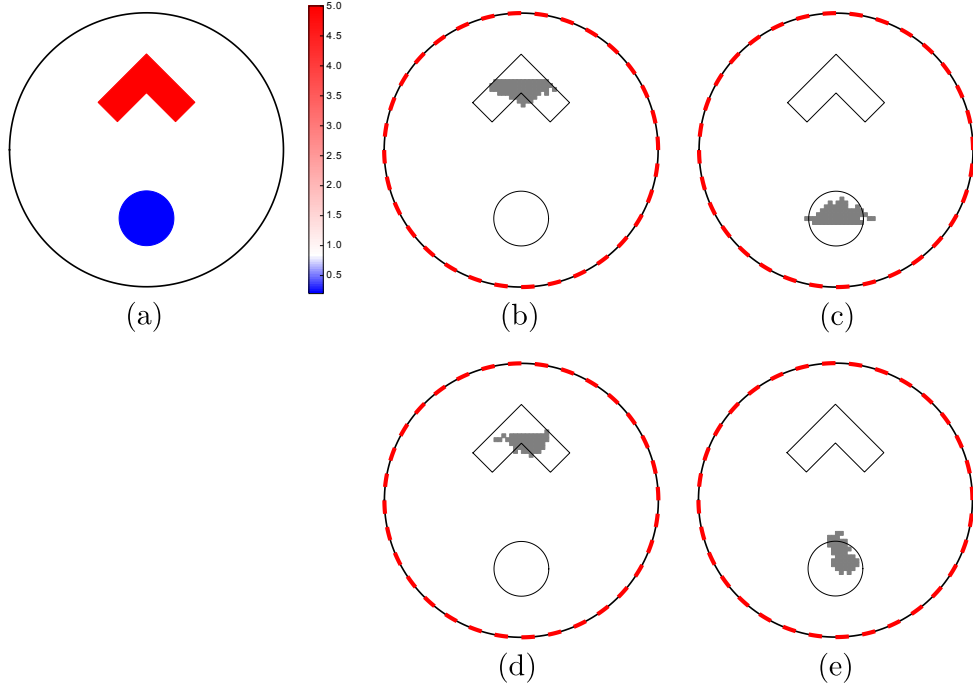


Fig. 4: (a) Two dimensional numerical phantom with positive part D_+ (wedge) and negative part D_- (ball). (b) Reconstruction of D_+ from noiseless datum with $\alpha_0 = 9.00 \times 10^{-4}$. (c) Reconstruction of D_- from noiseless datum with $\alpha_0 = 6.72 \times 10^{-4}$. (d) Reconstruction of D_+ with 0.5% noise and $\alpha_0 = 4.20 \times 10^{-3}$. (e) Reconstruction of D_- with 0.5% noise and $\alpha_0 = 3.26 \times 10^{-3}$.

where Id_k is the $k \times k$ identity matrix and $\mathbf{H} = \text{Id}_k - \frac{1}{k}\mathbf{1}_k$ is the orthogonal projection of \mathbb{R}^k onto \mathbb{R}_\diamond^k , i.e. $\mathbf{1}_k$ is the $k \times k$ matrix with 1 in each entry. Note that $\mathbf{R} = \mathbf{I}^T \mathbf{V}$ is the matrix representation of $R(\gamma)$ in the \mathbf{I} -basis, thus

$$\text{Sym}(\mathbf{I}^T \tilde{\mathbf{V}}) = \mathbf{R} + \text{Sym}(\mathbf{I}^T \mathbf{H} \mathbf{Y} \mathbf{V})$$

where Sym is the symmetric part of a matrix. We therefore write the noisy measurement as $\mathbf{R}^\delta = \mathbf{R} + \mathbf{N}^\delta$ with

$$\mathbf{N}^\delta = \delta \frac{\text{Sym}(\mathbf{I}^T \mathbf{H} \mathbf{Y} \mathbf{V})}{\|\text{Sym}(\mathbf{I}^T \mathbf{H} \mathbf{Y} \mathbf{V})\|_{\mathcal{L}(\mathbb{R}^k)}}.$$

For each $C \in \mathcal{A}$, let the $(k-1) \times (k-1)$ matrices \mathbf{B} and \mathbf{C} be representations of $R(\gamma_0)$ and $R'(\gamma_0)\chi_C$ by $\mathbf{B}_{i,j} = I^{(j)} \cdot R(\gamma_0)I^{(i)}$ and $\mathbf{C}_{i,j} = I^{(j)} \cdot R'(\gamma_0)[\chi_C]I^{(i)}$. We use the definiteness of the following matrices to check the monotonicity relations (cf. (2.10))

$$\begin{aligned} \mathbf{A}_+ &= \mathbf{R}^\delta - \mathbf{B} - \beta \mathbf{C}, \\ \mathbf{A}_- &= \mathbf{B} - \beta^U \mathbf{C} - \mathbf{R}^\delta. \end{aligned}$$

4.1. Numerical examples. A standard finite element (FE) method with piecewise affine elements is applied to evaluate the involved PDE problems for the measurement maps. In dimension two the unit disk domain will be considered with $k = 32$

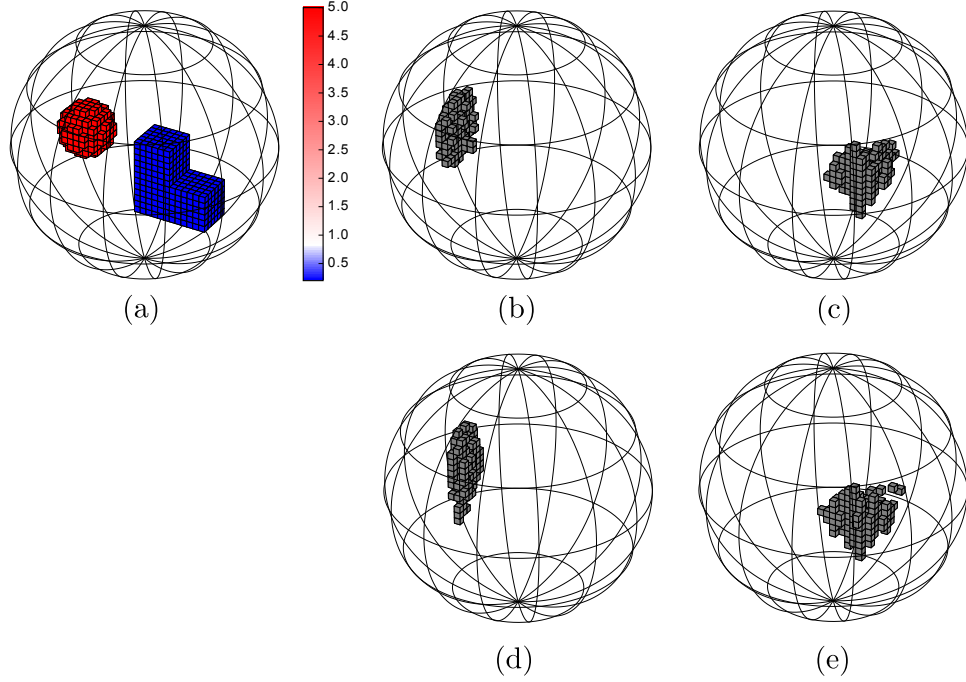


Fig. 5: (a) Three dimensional numerical phantom with positive part D_+ (ball) and negative part D_- (L-shape). (b) Reconstruction of D_+ from noiseless datum with $\alpha_0 = 7.50 \times 10^{-5}$. (c) Reconstruction of D_- from noiseless datum with $\alpha_0 = 2.90 \times 10^{-4}$. (d) Reconstruction of D_+ with 0.5% noise and $\alpha_0 = 2.40 \times 10^{-4}$. (e) Reconstruction of D_- with 0.5% noise and $\alpha_0 = 2.50 \times 10^{-4}$.

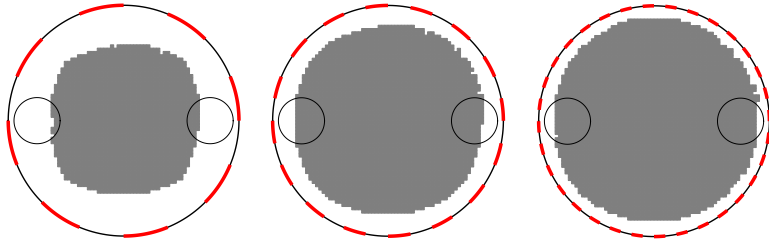


Fig. 6: For $k = 8, 16$, and 32 electrodes of size π/k , upper bounds of reconstructions of D_+ are shown, using regularization parameter $\alpha_0 = 0$. D_+ is the ball outlined on the right side of the domain and D_- is on the left.

electrodes of size π/k placed equidistantly on the boundary. In dimension three $k = 64$ almost equidistant electrodes, given as spherical caps of radius 0.1, will be placed on the unit sphere. For reconstruction we use a mesh with 8.0×10^4 and 1.6×10^5 nodes in two and three spatial dimensions, respectively. The mesh is more dense near the electrode positions to account for the weak singularities. For simulating the datum we use a different finer mesh which is also aligned with the inclusion boundaries for

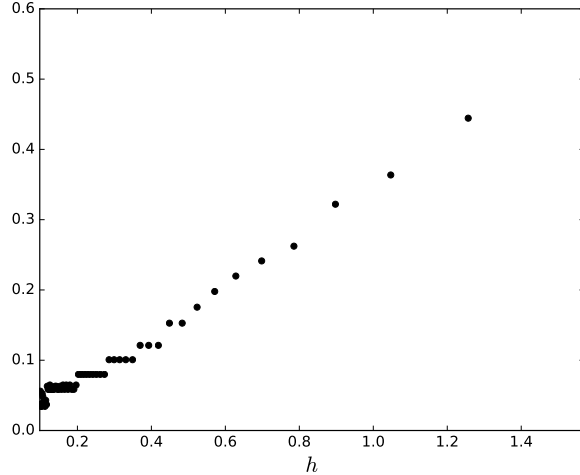


Fig. 7: For $k = 4, 5, \dots, 64$ electrodes of size π/k , the distance d_k from $\partial\Omega$ to upper bounds of reconstructions of D_+ is plotted (cf. Figure 6). $h = 2\pi/k$ is the corresponding maximal diameter from Theorem 3.3.

improved precision. The Fréchet derivative is evaluated using (A.4) on pixels and voxels with respective side length $\frac{1}{35}$ and $\frac{1}{20}$.

The conductivity $\gamma = 1 + 4\chi_{D_+} - \frac{4}{5}\chi_{D_-}$ will be used throughout, i.e. $\beta^L = \beta^U = 1$ and $\beta = 4$. The examples will include both reconstruction from a noiseless datum and from a noisy datum with 0.5% relative noise.

The reconstructions can be seen in Figure 3 and 4 in the two dimensional case, and in Figure 5 for the three dimensional case. As expected from Theorem 3.1, the CEM reconstructions are generally smaller than the actual inclusions, however, it is observed that the locations of positive and negative inclusions can be independently reconstructed with clear separation, and that the algorithm performs robustly under noisy measurements. As is typically the case with reconstructions from the CEM, the convex inclusions are easier to reconstruct compared to the non-convex, as seen by the wedge-shape and the L-shape in Figure 4 and 5, though the general position of the inclusions is correctly reconstructed. On a laptop with an Intel i7 processor with CPU clock rate of 2.4 GHz, each reconstruction is computed in an average of 0.15 seconds in two dimensions and 3.3 seconds in three dimensions.

From the numerical experiments we noted that the reconstructions are not very sensitive to the choice of the regularization parameter, which can be changed up to almost an order of magnitude with only minor changes in the reconstruction. This is in stark contrast to the definite case which is very sensitive to the regularization parameter choice [9]; this can be attributed the fact that test inclusions in the indefinite case are generally of significantly larger measure compared to the definite case, and the computations are therefore less sensitive to rounding errors.

On the other hand, it turns out that reconstruction based on the CEM can be difficult near the measurement boundary, and in fact there can be invisible inclusions close to $\partial\Omega$. This can be illustrated by computing reconstructions of inclusions close to the boundary with regularization parameter $\alpha_0 = 0$, which will give an upper bound to any reconstruction with non-zero regularization. From Figure 6 these upper

bounds are shown for $k = 8, 16$, and 32 electrodes, where it is observed that for $k = 8$ most of the inclusions will not be possible to reconstruct, and the distance d_k of the upper bound to $\partial\Omega$ depends on the number of electrodes. This experiment is repeated for $k = 4, 5, \dots, 64$ equidistant electrodes of size π/k , where in the sense of the extended electrodes in Theorem 3.3, we have $h = 2\pi/k$. Figure 7 suggests (up to the finite discretization) the conjecture that d_k is $O(h)$, meaning the same rate of convergence as the CEM to the CM in Theorem 3.3.

Even though the indefinite method and definite method ultimately are based on the same type of monotonicity relations, the cause of the methods' different behaviour with approximate models is, to the the authors' knowledge, an open problem.

5. Conclusions. We extended the regularization theory for the monotonicity method from the definite case to the indefinite case, and furthermore proved that positive and negative inclusions may be reconstructed separately by monotonicity-based reconstruction. For a regularization parameter choice criteria we proved that approximate forward models, including the CEM and SCEM, can be used in the monotonicity method, and the involved monotonicity relations converge to the exact solution from the CM as the approximation error and noise level decay.

We have presented a novel algorithm that implements the reconstruction method. Numerical examples, based on the CEM, provide evidence that the method is noise robust and capable of reconstructing inclusions with a realistic electrode model, provided that the inclusions are not too close to the measurement boundary.

Appendix A. Differentiability and monotonicity relations of the SCEM.

In this appendix we outline the usual Fréchet differentiability and monotonicity results for the SCEM that are well-known to hold for the standard CEM.

For the PDE problem (3.12)–(3.14), and the assumptions (3.11) for ζ , the weak formulation of the SCEM is for a weak solution pair $(v, V) \in H^1(\Omega) \oplus \mathbb{R}_\diamond^k$ [20],

$$(A.1) \quad \int_{\Omega} \gamma \nabla v \cdot \nabla w \, dx + \int_{\partial\Omega} \zeta(V - v)(W - w) \, dS = I \cdot W$$

for all $(w, W) \in H^1(\Omega) \oplus \mathbb{R}_\diamond^k$. The measurement map $R(\gamma)$ in (3.15) is clearly self-adjoint, since for $I_1, I_2 \in \mathbb{R}_\diamond^k$ with corresponding solution pairs (v_1, V_1) and (v_2, V_2) , then (A.1) implies,

$$I_2^T R(\gamma) I_1 = \int_{\Omega} \gamma \nabla v_2 \cdot \nabla v_1 \, dx + \int_{\partial\Omega} \zeta(V_2 - v_2)(V_1 - v_1) \, dS = I_1^T R(\gamma) I_2.$$

Now the monotonicity properties analogous to Proposition 2.1 can be shown.

PROPOSITION A.1. *For each $I \in \mathbb{R}_\diamond^k$ and two arbitrary conductivities $\gamma, \tilde{\gamma} \in L_+^\infty(\Omega)$ it holds*

$$(A.2) \quad \int_{\Omega} \frac{\tilde{\gamma}}{\gamma} (\gamma - \tilde{\gamma}) |\nabla \tilde{v}|^2 \, dx \leq I^T (R(\tilde{\gamma}) - R(\gamma)) I \leq \int_{\Omega} (\gamma - \tilde{\gamma}) |\nabla \tilde{v}|^2 \, dx$$

where (\tilde{v}, \tilde{V}) is the solution to (3.12)–(3.14) with conductivity $\tilde{\gamma}$ and current pattern I . The same contact impedance ζ is used for both measurement maps.

Proof. Let (v, V) be the solution pair for γ , and denote by B and \tilde{B} the bilinear

forms in (A.1) for γ and $\tilde{\gamma}$, respectively. Now (A.1) entails

$$\begin{aligned}
 I^T(R(\tilde{\gamma}) - R(\gamma))I &= I^T((\tilde{V} - V) + \tilde{V} - \tilde{V}) \\
 &= B((v, V), (\tilde{v} - v, \tilde{V} - V)) + B((v, V), (\tilde{v}, \tilde{V})) - \tilde{B}((\tilde{v}, \tilde{V}), (\tilde{v}, \tilde{V})) \\
 (A.3) \quad &= - \int_{\Omega} \gamma |\nabla(v - \tilde{v})|^2 dx + \int_{\Omega} (\gamma - \tilde{\gamma}) |\nabla \tilde{v}|^2 dx \\
 &\quad - \int_{\partial\Omega} \zeta |(v - V) - (\tilde{v} - \tilde{V})|^2 dS \\
 &\leq \int_{\Omega} (\gamma - \tilde{\gamma}) |\nabla \tilde{v}|^2 dx
 \end{aligned}$$

which proves the second inequality in (A.2). Using (A.3), with γ and $\tilde{\gamma}$ swapped, proves the first inequality of (A.2),

$$\begin{aligned}
 I^T(R(\tilde{\gamma}) - R(\gamma))I &= -I^T(R(\gamma) - R(\tilde{\gamma}))I \\
 &= \int_{\Omega} \tilde{\gamma} |\nabla(v - \tilde{v})|^2 dx + \int_{\Omega} (\gamma - \tilde{\gamma}) |\nabla v|^2 dx \\
 &\quad + \int_{\partial\Omega} \zeta |(v - V) - (\tilde{v} - \tilde{V})|^2 dS \\
 &= \int_{\Omega} \gamma |\nabla v - \frac{\tilde{\gamma}}{\gamma} \nabla \tilde{v}|^2 dx + \int_{\Omega} \frac{\tilde{\gamma}}{\gamma} (\gamma - \tilde{\gamma}) |\nabla \tilde{v}|^2 dx \\
 &\quad + \int_{\partial\Omega} \zeta |(v - V) - (\tilde{v} - \tilde{V})|^2 dS \\
 &\geq \int_{\Omega} \frac{\tilde{\gamma}}{\gamma} (\gamma - \tilde{\gamma}) |\nabla \tilde{v}|^2 dx,
 \end{aligned}$$

thus concluding the proof. \square

Clearly the SCEM satisfies the simple monotonicity relation

$$\gamma \geq \tilde{\gamma} \text{ a.e. in } \Omega \implies R(\tilde{\gamma}) \geq R(\gamma).$$

Finally, we show that the forward map $\gamma \mapsto R(\gamma)$ of the SCEM is Fréchet differentiable.

PROPOSITION A.2. *The map $\gamma \mapsto R(\gamma)$ is Fréchet differentiable at $\gamma \in L_+^\infty(\Omega)$ in $L^\infty(\Omega)$ with derivative*

$$(A.4) \quad I_2^T R'(\gamma)[\eta] I_1 = - \int_{\Omega} \eta \nabla v_2 \cdot \nabla v_1 dx, \quad \eta \in L^\infty(\Omega),$$

where for $j \in \{1, 2\}$, (v_j, V_j) is the solution pair to (3.12)–(3.14) with conductivity γ and current pattern $I_j \in \mathbb{R}_\diamond^k$.

Proof. We denote the corresponding solution pairs for conductivity $\gamma + \eta$ by (v_j^η, V_j^η) for $j \in \{1, 2\}$. Using that $R(\gamma + \eta)$ is self-adjoint and the weak form in (A.1),

$$\begin{aligned}
 I_2^T(R(\gamma) - R(\gamma + \eta))I_1 &= I_2^T R(\gamma) I_1 - I_2^T R(\gamma + \eta) I_2 \\
 &= \int_{\Omega} (\gamma + \eta) \nabla v_2^\eta \cdot \nabla v_1 dx + \int_{\partial\Omega} \zeta (V_2^\eta - v_2^\eta)(V_1 - v_1) dS \\
 &\quad - \int_{\Omega} \gamma \nabla v_1 \cdot \nabla v_2^\eta dx - \int_{\partial\Omega} \zeta (V_1 - v_1)(V_2^\eta - v_2^\eta) dS \\
 (A.5) \quad &= \int_{\Omega} \eta \nabla v_2^\eta \cdot \nabla v_1 dx.
 \end{aligned}$$

Thus, (A.4) and (A.5) give the estimate

$$(A.6) \quad |I_2^T(R(\gamma) + R'(\gamma)\eta - R(\gamma + \eta))I_1| \leq \|\eta\|_{L^\infty(\Omega)} \|\nabla v_1\|_{L^2(\Omega)} \|\nabla(v_2^\eta - v_2)\|_{L^2(\Omega)}.$$

Define $(\psi, \Psi) = (v_2^\eta - v_2, V_2^\eta - V_2)$. From (A.1) then (ψ, Ψ) satisfies

$$(A.7) \quad \int_{\Omega} (\gamma + \eta) \nabla \psi \cdot \nabla w \, dx + \int_{\partial\Omega} \zeta(\Psi - \psi)(W - w) \, dS = - \int_{\Omega} \eta \nabla v_2 \cdot \nabla w \, dx$$

for all $(w, W) \in H^1(\Omega) \oplus \mathbb{R}_\diamond^k$. Since $\gamma \in L_+^\infty(\Omega)$ then $\inf(\gamma) \geq 2c > 0$ for a positive constant c . Now assume $\|\eta\|_{L^\infty(\Omega)} \leq c$, i.e., $\inf(\gamma + \eta) \geq c > 0$ independently of η , and choose $(w, W) = (\psi, \Psi)$ in (A.7),

$$\begin{aligned} c \|\nabla \psi\|_{L^2(\Omega)}^2 &\leq \int_{\Omega} (\gamma + \eta) |\nabla \psi|^2 \, dx + \int_{\partial\Omega} \zeta |\Psi - \psi|^2 \, dS \\ &= - \int_{\Omega} \eta \nabla v_2 \cdot \nabla \psi \, dx \\ (A.8) \quad &\leq \|\eta\|_{L^\infty(\Omega)} \|\nabla v_2\|_{L^2(\Omega)} \|\nabla \psi\|_{L^2(\Omega)}. \end{aligned}$$

$\|\nabla v_j\|_{L^2(\Omega)} \leq C \|I_j\|_2$ by continuous dependence on I_j [20, Theorem 2.2], which in combination with (A.6) and (A.8) concludes the proof,

$$|I_2^T(R(\gamma) + R'(\gamma)\eta - R(\gamma + \eta))I_1| \leq C \|\eta\|_{L^\infty(\Omega)}^2 \|I_1\|_2 \|I_2\|_2,$$

in particular

$$\frac{\|R(\gamma) + R'(\gamma)\eta - R(\gamma + \eta)\|_{\mathcal{L}(\mathbb{R}_\diamond^k)}}{\|\eta\|_{L^\infty(\Omega)}} \leq C \|\eta\|_{L^\infty(\Omega)} \rightarrow 0 \text{ for } \|\eta\|_{L^\infty(\Omega)} \rightarrow 0.$$

Hence R is Fréchet differentiable at $\gamma \in L_+^\infty(\Omega)$ in direction $\eta \in L^\infty(\Omega)$ with derivative $R'(\gamma)\eta$. \square

REFERENCES

- [1] A. ABUBAKAR, T. M. HABASHY, M. LI, AND J. LIU, *Inversion algorithms for large-scale geophysical electromagnetic measurements*, Inverse Problems, 25 (2009). Article ID 123012.
- [2] L. BORCEA, *Electrical impedance tomography*, Inverse Problems, 18 (2002), pp. 99–136.
- [3] T. BRANDER, M. KAR, AND M. SALO, *Enclosure method for the p -Laplace equation*, Inverse Problems, 31 (2015). Article ID 045001.
- [4] M. BRÜHL, *Explicit characterization of inclusions in electrical impedance tomography*, SIAM Journal on Mathematical Analysis, 32 (2001), pp. 1327–1341.
- [5] M. BRÜHL AND M. HANKE, *Numerical implementation of two non-iterative methods for locating inclusions by impedance tomography*, Inverse Problems, 16 (2000), pp. 1029–1042.
- [6] M. CHENEY, D. ISAACSON, AND J. C. NEWELL, *Electrical impedance tomography*, SIAM Review, 41 (1999), pp. 85–101.
- [7] H. GARDE, *Comparison of linear and non-linear monotonicity-based shape reconstruction using exact matrix characterizations*, To appear in Inverse Problems in Science and Engineering, (2017).
- [8] H. GARDE AND K. KNUDSEN, *Distinguishability revisited: depth dependent bounds on reconstruction quality in electrical impedance tomography*, SIAM Journal on Applied Mathematics, 77 (2017), pp. 697–720.
- [9] H. GARDE AND S. STABOULIS, *Convergence and regularization for monotonicity-based shape reconstruction in electrical impedance tomography*, Numerische Mathematik, 135 (2017), pp. 1221–1251.
- [10] B. GEBAUER, *Localized potentials in electrical impedance tomography*, Inverse Problems and Imaging, 2 (2008), pp. 251–269.

- [11] N. GRINBERG AND A. KIRSCH, *The factorization method for obstacles with a-priori separated sound-soft and sound-hard parts*, Mathematics and Computers in Simulation, 66 (2004), pp. 267–279.
- [12] M. HANKE AND M. BRÜHL, *Recent progress in electrical impedance tomography*, Inverse Problems, 19 (2003), pp. S65–S90. Special section on imaging.
- [13] M. HANKE-BOURGEOIS AND A. KIRSCH, *Sampling methods*, in *Handbook of Mathematical Methods in Imaging*, Springer, 2015, pp. 591–647.
- [14] B. HARRACH AND M. N. MINH, *Enhancing residual-based techniques with shape reconstruction features in electrical impedance tomography*, Inverse Problems, 32 (2016). Article ID 125002.
- [15] B. HARRACH AND M. ULLRICH, *Monotonicity-based shape reconstruction in electrical impedance tomography*, SIAM Journal on Mathematical Analysis, 45 (2013), pp. 3382–3403.
- [16] ———, *Resolution guarantees in electrical impedance tomography*, IEEE Transactions on Medical Imaging, 34 (2015), pp. 1513–1521.
- [17] D. S. HOLDER, ed., *Electrical impedance tomography; methods, history, and applications*, IOP publishing Ltd., 2005.
- [18] N. HYVÖNEN, *Complete electrode model of electrical impedance tomography: Approximation properties and characterization of inclusions*, SIAM Journal on Applied Mathematics, 64 (2004), pp. 902–931.
- [19] ———, *Approximating idealized boundary data of electric impedance tomography by electrode measurements*, Mathematical Models and Methods in Applied Sciences, 19 (2009), pp. 1185–1202.
- [20] N. HYVÖNEN AND L. MUSTONEN, *Smoothed complete electrode model*, Preprint available from <https://arxiv.org/abs/1703.08022>, (2017).
- [21] M. IKEHATA, *How to draw a picture of an unknown inclusion from boundary measurements. Two mathematical inversion algorithms*, Journal of Inverse and Ill-Posed Problems, 7 (1999), pp. 255–271.
- [22] ———, *Reconstruction of the support function for inclusion from boundary measurements*, Journal of Inverse and Ill-Posed Problems, 8 (2000), pp. 367–378.
- [23] ———, *A regularized extraction formula in the enclosure method*, Inverse problems, 18 (2002), pp. 435–440.
- [24] K. KARHUNEN, A. SEPPÄNEN, A. LEHIKOINEN, J. BLUNT, J. P. KAIPIO, AND P. J. M. MONTEIRO, *Electrical resistance tomography for assessment of cracks in concrete*, Materials Journal, 107 (2010), pp. 523–531.
- [25] K. KARHUNEN, A. SEPPÄNEN, A. LEHIKOINEN, P. J. M. MONTEIRO, AND J. P. KAIPIO, *Electrical resistance tomography imaging of concrete*, Cement and Concrete Research, 40 (2010), pp. 137–145.
- [26] A. KIRSCH AND N. GRINBERG, *The factorization method for inverse problems*, Oxford University Press, USA, 2008.
- [27] A. LECHLEITER, *A regularization technique for the factorization method*, Inverse problems, 22 (2006), pp. 1605–1625.
- [28] A. LECHLEITER, N. HYVÖNEN, AND H. HAKULA, *The factorization method applied to the complete electrode model of impedance tomography*, SIAM Journal on Applied Mathematics, 68 (2008), pp. 1097–1121.
- [29] S. SCHMITT, *The factorization method for EIT in the case of mixed inclusions*, Inverse Problems, 25 (2009). Article ID 065012.
- [30] E. SOMERSALO, M. CHENEY, AND D. ISAACSON, *Existence and uniqueness for electrode models for electric current computed tomography*, SIAM Journal on Applied Mathematics, 52 (1992), pp. 1023–1040.
- [31] A. TAMBURRINO, *Monotonicity based imaging methods for elliptic and parabolic inverse problems*, Journal of Inverse and Ill-posed Problems, 14 (2006), pp. 633–642.
- [32] A. TAMBURRINO AND G. RUBINACCI, *A new non-iterative inversion method for electrical resistance tomography*, Inverse Problems, 18 (2002), pp. 1809–1829.
- [33] L. N. TREFETHEN AND M. EMBREE, *Spectra and Pseudospectra: The Behavior of Nonnormal Matrices and Operators*, Princeton University Press, Princeton, NJ, 2005.
- [34] G. UHLMANN, *Electrical impedance tomography and Calderón’s problem*, Inverse Problems, 25 (2009). Article ID 123011.
- [35] T. YORK, *Status of electrical tomography in industrial applications*, Journal of Electronic Imaging, 10 (2001), pp. 608–619.